

The discovery and maturation of peptide biologics targeting the small G protein Cdc42: a bioblockade for Ras-driven signalling

George J. N. Tetley<sup>†¶</sup>, Natasha P. Murphy<sup>†</sup>, Stephane Bonetto<sup>‡§</sup>, Gabriela Ivanova-Berndt<sup>‡¶</sup>, Jefferson Revell<sup>#</sup>, Helen R. Mott<sup>†\*</sup>, R. Neil Cooley<sup>‡‡</sup> and Darerca Owen<sup>†\*</sup>

From the <sup>†</sup>Department of Biochemistry, University of Cambridge, 80 Tennis Court Road, Cambridge. CB2 1GA. U.K.; <sup>‡</sup>Isogenica Ltd., Chesterford Research Park, Little Chesterford, Essex. CB10 1XL. U.K.; <sup>#</sup>MedImmune, Sir Aaron Klug Building, Granta Park, Cambridge CB21 6GH. U.K.

Running Title: Inhibition of Ras-Cdc42 signalling by a cyclic peptide

<sup>¶</sup>Present address: Deep Science Ventures, 51 Eastcheap, London, EC3M 1JP. U.K.

<sup>§</sup>Present address: Agenus UK Ltd, 315 Science Park, Milton Road, Cambridge, CB4 0WG. U.K.

<sup>¶</sup>Present address: Bicycle Therapeutics Limited, B900, Babraham Research Campus, Cambridge, CB22 3AT. U.K.

<sup>‡</sup>Present address: Abzena, Babraham Research Campus, Babraham, Cambridge CB22 3AT. U.K.

\*To whom correspondence should be addressed: Darerca Owen, Department of Biochemistry, University of Cambridge, 80 Tennis Court Road, Cambridge. CB2 1GA. U.K. Tel.: 44-1223-764824; Fax: 44-1223-766002; E-mail:do202@cam.ac.uk; Helen R. Mott, Department of Biochemistry, University of Cambridge, 80 Tennis Court Road, Cambridge. CB2 1GA. U.K. Tel.: 44-1223-764825; Fax: 44-1223-766002; E-mail: hrm28@cam.ac.uk

**Keywords:** cancer, CDC42, cell migration, cell signaling, cell proliferation, cyclic peptide, drug discovery, KRas, NMR, peptide conformation

---

## ABSTRACT

Aberrant Ras signalling drives 30% of cancers and inhibition of Rho family small-GTPase signalling has been shown to combat Ras-driven cancers. Here we present the discovery of a 16mer cyclic peptide that binds to Cdc42 with nanomolar affinity. Affinity maturation of this sequence has produced a panel of derived candidates with increased affinity and modulated specificity for other closely related small-GTPases. The structure of the tightest binding peptide was solved by NMR and its binding site on Cdc42 determined. Addition of a cell penetrating sequence allowed

the peptides to access the cell interior and engage with their target(s), modulating signalling pathways. In Ras-driven cancer cell models, the peptides have an inhibitory effect on proliferation and show suppression of both invasion and motility. As such they represent promising candidates for Rho-family small GTPase inhibitors and therapeutics targeting Ras-driven cancers. Our data adds to the growing literature demonstrating that peptides are establishing their place in the biologics arm of drug discovery.

Aberrant signalling from the small G protein Ras has been shown to drive approximately one third of all human cancers making it a compelling therapeutic target (1). Targeting Ras isoforms directly has proven difficult historically, although some progress has been made recently (2-4). Cdc42, together with Rac1, RhoA and other members of the Rho family small GTPases, is a key regulator of the actin cytoskeleton and therefore cell architecture and motility (reviewed in (5)). Cdc42 is often found to signal downstream of the master regulator, Ras, and induces the formation of filopodia by initiating actin remodeling, which is key to cell motility. Deregulation of Cdc42, therefore, results in the progression of several disease states, including tumour metastasis (6). Genetic deletion of Cdc42 in Ha-Ras G12V-transformed fibroblasts results in a significant block in cell cycle progression and therefore in cell proliferation, demonstrating an essential role of Cdc42 in Ras-induced transformation (7). Correspondingly, overexpression of Cdc42 is implicated in several human cancers where it correlates with poor prognosis (8-10). Although mutations in Cdc42 are rarely found in human cancers, oncogenic mutations have been extensively characterized in its regulators *e.g.* the GEFs Dbl (11) and Asef2 (12) and the GAP, DLC1 (13). Cdc42 participates in both physiological and tumorigenic processes by interacting with its effector proteins. One such family of effectors, the CRIB proteins, includes activated Cdc42-associated kinase (ACK), the p21 activated kinases (PAKs) and Wiskott-Aldrich syndrome proteins (WASPs)(14).

Inhibition of Cdc42 has been demonstrated to reverse the oncogenic properties of v-Ha-Ras transformed cells in experiments employing the 42 amino acid G protein binding region (GBD) of ACK, a previously mentioned Cdc42 effector (15). This peptide binds to Cdc42 at a binding surface which prevents it interacting with its downstream effector proteins, all of which employ overlapping

#### *Inhibition of Ras-Cdc42 signalling by a cyclic peptide*

binding surfaces on Cdc42 (16). This inhibits Cdc42-driven signalling pathways, which must be necessary for transformation by Ras in this model.

This observation, together with our structural and biophysical analysis of the Cdc42-ACK GBD complex (17,18) prompted us to undertake a peptide discovery campaign, using CIS display technology, to identify a Cdc42 binding peptide that would similarly inhibit effector interaction and Ras-driven oncogenesis but would possess properties more compatible with future use as a lead therapeutic. CIS display is a biological display technology that links the DNA coding sequence of library members directly to the encoded peptide in a cell-free system by employing the binding properties of the R1 RepA protein to the origin of replication *i.e.* the cis-binding activity of the protein to its coding DNA (19). The technology allows generation and interrogation of the very large library sizes (routinely  $10^{13}$  library members) associated with cell-free display and offers greater stability than many orthogonal methods (for example ribosome or RNA display) by employing DNA and the robust CIS RepA system.

Despite the knowledge for over 30 years that targeting Ras and other small G proteins would have enormous therapeutic potential, multiple issues have been encountered in attempts to attack them (20). Small G-proteins all contain a conserved G domain comprising five  $\alpha$  helices surrounding a six-stranded  $\beta$  sheet (21) This architecture mediates binding to  $Mg^{2+}$  and either GTP or GDP, with GTP binding associated with activation. The picomolar affinity for guanine nucleotides together with the ubiquitous nature of guanine nucleotide usage and cellular abundance has prevented the development of small molecule therapeutics based on inhibition of nucleotide binding (22). Likewise the relatively smooth surface of the small G proteins has also confounded searches for small molecule

therapeutics due to the lack of other binding pockets, although some progress has been made in this regard in recent years (23).

Peptides and their orthologues can bind surfaces of proteins inhospitable to small molecules and as such can inhibit protein-protein interactions successfully, with the added property of exquisite specificity. Thus, peptides or peptidomimetics provide an opportunity to mimic the effect of ACK GBD overexpression, which was effective in inhibiting transformation in oncogenic NIH3T3 cells (15) by allowing targeting of the functional face of the Cdc42. Peptide therapeutic candidates have traditionally suffered from poor delivery and stability, however progress on both fronts continues to be made, using cell penetrating peptides (CPPs)(24) and delivery vehicles (25) and introducing unnatural modifications into peptide structures (26-29), allowing peptide biologics to join the current repertoire of therapeutics (30).

Here we report the identification and maturation of a lead 16mer cyclic peptide using CIS display (19) to produce a panel of cyclic peptides that bind Cdc42 with low nanomolar affinity. Binding has been characterized by biophysical methods, indicating the docking site on Cdc42 and demonstrating varying selectivity between peptides and related small GTPases. The peptides are shown to have promising phenotypic effects in cells when linked to a nona-arginine motif facilitating entry; reducing proliferation and particularly inhibiting motility and invasion. These peptides provide a promising lead platform for development of a therapeutic peptidomimetic targeting Rho-family signalling and therefore preventing oncogenesis in Ras-driven cancers.

## Results

### CIS display biopanning

Selections were performed following the work plan detailed in (19). Ten naïve peptide libraries,

### *Inhibition of Ras-Cdc42 signalling by a cyclic peptide*

encoding peptides 10-25 amino acids long were separated into three pools: short linear (SL) (10 and 12mer), long linear (LL) (16, 20 and 25mer) and cyclic (C) (14, 15, 16, 17 and 18mer) and selected against Cdc42·GMPPNP. The five libraries in the cyclic pool contained two constant cysteines (at positions N+4 and C-4) designed to allow production of disulphide-linked cyclic peptides under non-reducing conditions. Two methods of elution were used in parallel for each library pool: heating to 75° C or competition with the ACK GBD peptide, generating six individual selections. Competition with the ACK GBD was designed to select for peptides that bind to an interface on Cdc42 that overlaps with that of ACK. After four rounds of biopanning DNA recovery significantly increased (data not shown), indicating binding peptide enrichment. Next generation sequence analysis of the peptide coding DNA indicated three highly enriched peptides (which each represented over 20% of recovered sequences), two from the short linear and one from the cyclic library pools, as shown in Figure 1A. The three selection pools showed different patterns of enrichment. In the long linear libraries individual sequences are hydrophobic, suggestive of less specific binders, with no dominant motif. In contrast the short linear pool produced a highly dominant motif (HISWPXN) in both heat and competitive elution experiments while in the cyclic libraries one sequence (C1) was strongly enriched, especially under competitive elution conditions where it comprised ~70% of the recovered sequences. Several of the more frequently occurring alternative sequences selected from the short linear and cyclic libraries were single site variants stemming from the dominant sequence. No strong homology was shared across the cyclic and short linear consensus sequences.

### Peptide validation

Phage display of the three most highly selected sequences was used to validate peptide specificity for Cdc42 in an ELISA assay, as well as testing the

nucleotide dependence of the interaction. Results for the three dominant sequences, C1, SL1 and SL2, are shown in Figure 1B. SL2 bound strongly but non-specifically to all the proteins tested, including the negative control, BSA. SL1 gave weaker signals, which were again non-specific. C1 however generated strong signals with Cdc42·GMPPNP and low signals with Cdc42·GDP, RalB·GMPPNP and BSA. Some binding between C1 and Rac1·GMPPNP was also observed. These data suggested that, among these targets, C1 was specific for Cdc42·GMPPNP.

Quantitative peptide binding affinities were next determined by competition with the Cdc42-ACK GBD complex in scintillation proximity assays (SPAs). Peptide solubility at pH7.5 (<200  $\mu\text{M}$ ) tended to limit the concentration in the assays, such that the SL1 and SL2 peptides did not produce full competition data and could not be fitted (data not shown). C1 however, inhibited the Cdc42·GMPPNP-ACK GBD interaction with a  $K_d$  of 350nM (Figure 1C). The competition observed did not go to completion, i.e. the signal due to Cdc42-ACK GBD did not reach zero, suggesting that the binding site for C1 on Cdc42 partially overlaps with the ACK-Cdc42 interaction surface. Interestingly the affinity of C1 for Cdc42·GMPPNP was also shown to be dependent on the disulphide bond in the cyclic peptide, since addition of 50mM DTT or mutation of the cysteine residues to serine lowered the binding affinity significantly (Figure 1C).

### **C1 validation in cells**

The C1 sequence was re-synthesized with the addition of a C-terminal nona-arginine motif (9R) to facilitate cell penetration and an N-terminal linked FAM (carboxyfluorescein) group for visualization. The binding of this modified peptide to Cdc42 was confirmed by fluorescence polarization (FP) and the results are shown in Figure 2A. Direct binding of Cdc42·GMPPNP to

### *Inhibition of Ras-Cdc42 signalling by a cyclic peptide*

the FAM-C1-9R peptide gave a dissociation constant of  $0.36 \pm 0.09 \mu\text{M}$  (upper panel). The binding of FAM-9R was so low it could not be accurately determined. The  $K_d$  of untagged C1 for Cdc42·GMPPNP in competition FP was determined to be  $1.61 \pm 0.44 \mu\text{M}$  (Figure 2A, lower panel), indicating that the addition of 9R and FAM did not adversely affect Cdc42 binding *in vitro*. The very low affinity of FAM-9R for Cdc42 suggest that the slight difference in affinity between FAM-C1-9R and C1 may just reflect technical differences in the experimental methodologies.

To assess peptide entry into cells, mouse embryo fibroblasts (MEFs), were incubated in media containing FAM-C1-9R at concentrations from 60 nM to 10  $\mu\text{M}$  for between 2 and 5 hours at 37 °C before being washed and imaged by live cell confocal microscopy. Figure 2B shows images of cells exposed to 10  $\mu\text{M}$  peptide compared with a 5  $\mu\text{M}$  peptide treatment and a FITC control. At peptide concentrations of 10  $\mu\text{M}$  the MEFs showed signs of membrane disruption and cell death. Neither the 5 $\mu\text{M}$  peptide or the FITC-treated cells show such atypical cells at the time-points observed. This data corroborates previous observations of a toxicity threshold for the nona-arginine CPP (31) and therefore 5  $\mu\text{M}$  FAM-C1-9R was the maximum concentration used in subsequent experiments. Example images for treatments with  $\leq 5 \mu\text{M}$  peptide in Figure 2C show that the peptide can access the cell interior at a variety of concentrations and within 2 hours of dosing. The cells in these images appear healthy with the majority of the peptide dispersed in a punctate pattern in the cytoplasm, suggesting an endosomal location, as is often seen with peptides (32,33). The cytosol and nuclei of the cells however, show fluorescence above background levels, suggesting that not all peptide is confined to endosomes and that endosomal exit has allowed a wider distribution in the cells.

Next we investigated the effects of FAM-C1-9R on relevant cell signalling pathways. As our ultimate aim was to engineer peptide inhibitors of Cdc42 in order to attack Ras-driven cancers, we chose to examine signalling pathways using MEFs derived from four mice, two of which carried a Cre-induced G12D oncogenic K-Ras mutant (34). Previous work in our laboratory (our unpublished results) and from others (35,36) has shown Stat3 Tyr705 is a target for phosphorylation downstream of ACK, so pTyr705 Stat3 was chosen as a readout for an active Cdc42-ACK signalling pathway. Cells were treated with 1  $\mu$ M FAM-C1-9R for 1 and 24 hours alongside untreated controls. Four different MEF isolates were used from four littermates: A and C expressing G12D K-Ras, B and D expressing wild-type K-Ras. Figure 2D shows pTyr705 Stat3 levels demonstrating a marked decrease at one hour in cell lines A, B and D, returning to untreated levels by the 24 hour time-point, while total Stat3 remained relatively constant, demonstrating a reduction in signalling by Cdc42 on exposure to FAM-C1-9R. ERK phosphorylation was also probed, to assess activity through the MAPK pathway and results are shown in Figure 2D. MEK induces phosphorylation of ERK1/2 at residues threonine 202 and tyrosine 204, so levels of pThr202/pTyr204 ERK1/2 were analysed. Suppression of pThr202/pTyr204 ERK1/2 phosphorylation is visible at 1 hour for cells lines A and B, although not in cell lines C and D, suggesting that the MAPK pathway, downstream of Ras, can be affected by FAM-C1-9R.

Taken together, these data demonstrate that FAM-C1-R9 enters cells, likely by an endosomal route but can escape into other parts of the cell, where it is able to elicit the signalling effects that it was designed to accomplish.

### **Maturation of C1**

Although CIS display offers the potential to

### *Inhibition of Ras-Cdc42 signalling by a cyclic peptide*

interrogate some of the largest naïve sequence space available, the naïve 16mer library used in the original selections covers only approximately 0.0125% of possible sequences, suggesting the likelihood that other potentially higher affinity sequences could exist that had not been available for selection. Thus a maturation library designed to search the sample space around the C1 sequence was constructed and selected against Cdc42·GMPPNP. Sequence analysis of the selected peptides, after 4 rounds of biopanning, showed that residue replacement was favoured at 6 positions whereas 3 other positions saw no substitutions highlighting their possible key roles in the target engagement. The fold enhancement of individual amino acids at these positions compared to the initial library are shown in Figure 3A. A panel of peptides was then synthesized, based on the enriched sequences observed in the NGS analysis of the selections, to represent the most favourable residue replacements, as shown in Figure 3B. Binding affinities for this panel of peptides were determined by competition SPA, as described above and dissociation constants are listed in Figure 3B with representative data shown in Figure 3C. For five of these second generation peptides, the affinity for Cdc42 was increased significantly (5-20-fold) and reached values close to the affinity of the complete ACK GBD for Cdc42 (20-30 nM), lending further promise for their ability to act as competitive inhibitors of Cdc42 effector proteins in cells.

The maturation data suggest that the combined H8R, G10D substitutions in peptide candidates are important for increasing binding affinity, as all peptides with these substitutions have an affinity of 32 nM or lower for Cdc42. Effects of other replacements are less clear, however the combined effect of P1T, H8Q and Q16R are favourable in P1 and P9.

### **Mode of peptide binding to Cdc42**

One of the second generation peptides with the

tightest binding, P7, was chosen for structural analysis by NMR.  $^{15}\text{N}$ -HSQC spectra of Cdc42 were recorded and the chemical shifts of the backbone amides were monitored with increasing P7 peptide concentrations (Figure 4A). Most of the peaks in the Cdc42 spectrum that experienced chemical shift changes were in slow exchange, so that peaks corresponding to both the free and bound species were observable in the intermediate timepoints of the titration. Residues, whose peaks in the complex spectrum could be assigned and whose chemical shift changes were higher than average, were identified (Supplementary Figure 1). To these were added those residues whose peaks had moved too far from their position in the free Cdc42 spectrum to be reliably assigned (labelled in blue in Figure 4A). The residues with significant shift changes and which are solvent accessible are shown mapped onto the Cdc42 structure in Figure 4B. Chemical shift perturbations can indicate that a particular residue is involved in the interface with the binding partner, but may also be due to longer-range allosteric effects. Residues that are not accessible to the solvent are unlikely to be involved in direct interactions and their removal reduces the number of indirect contributions to chemical shift mapping. The chemical shift mapping localizes the P7 binding site to a face of Cdc42 that is involved in binding to a critical section of the N-termini of the GBDs of effector proteins (18,37).

The structure of the P7 peptide in isolation was determined by NMR. The peptide was fully assigned using standard homonuclear experiments and the NOESY was used to generate 440 unique distance restraints. The RMSD of the final, water-refined structures is  $0.37\text{\AA}$  over all backbone atoms and the large number of distance restraints mean that the structure is well defined (Table 1). The disulphide bond, in combination with the presence of two proline residues within the middle of sequence, which lend rigidity, means that the peptide adopts a tightly constrained structure

#### *Inhibition of Ras-Cdc42 signalling by a cyclic peptide*

(Figure 4C and D). Stacking interactions between the three aromatic residues within the sequence (Trp11, Trp14, Tyr15) further stabilize the structure. There is no regular secondary structure in the peptide, which merely forms a series of turns. The overall structure forms a single turn of a loose, irregular, left-handed helix between residues 3 and 15, pinned by the disulphide bond between Cys4 and Cys13, with the N- and C-termini protruding out on opposite sides (Figure 4C). Arg8 and Asp10, which drive higher binding affinities, are displayed on a loop opposite the disulphide bond, which presumably constitutes the Cdc42 binding face. (Figure 4D) The structure explains why the disulphide bond is necessary for high affinity binding to Cdc42, since there is only one residue, Val6, in its hydrophobic core (Figure 4C). Without the disulphide, therefore, this compact structure would not form stably and would be unable to display the Cdc42 binding face correctly.

Data-driven docking (HADDOCK) was next used to predict the structure of the Cdc42-P7 complex (38,39). The NMR chemical shift mapping was used to determine the active residues in Cdc42 and the matured peptide sequences and affinity measurements (Figure 3B) were used to determine the active residues in the peptide (Arg8 and Asp10). The complete Cdc42-P7 docked model is shown in Figure 5A and B and identifies both hydrophobic and polar interactions between Cdc42 and P7. In particular, the conserved peptide residues Trp11 and Tyr15 (found in all second generation peptides except P9) form the hydrophobic core of interactions with a Cdc42 pocket between strand  $\beta 1$  and helices  $\alpha 1$  and  $\alpha 5$ . This pocket is lined by Cdc42 residues such as Val42, Val44 and Tyr23. Tyr15 is also close to Cdc42 residues Thr25 and Asn26, which could make polar interactions with the Tyr OH group. Arg8 and Asp10 are predicted to form a salt bridge with each other in the free peptides but Asp10 is within  $3\text{\AA}$  of Lys166<sup>Cdc42</sup> in the model and hence may form a salt bridge. Arg8 is within  $3\text{\AA}$  of

Tyr23<sup>Cdc42</sup> and potentially could form a hydrogen bond (Figure 5C), although the backbone amide of Tyr23<sup>Cdc42</sup> did not show chemical shift changes when the peptide bound. The Cdc42 pocket that binds to P7 also contacts the N-terminus of the ACK GBD in the Cdc42-ACK complex (Figure 6). This is consistent with the previous observation that P7 can compete with ACK GBD binding to Cdc42 (Figure 1C), which implies overlapping binding sites. Importantly this region of Cdc42 contributes significantly thermodynamically to the binding of both ACK and WASP (18,37) and is also demonstrated to bind the other known CRIB effectors PAK1 and Par6 where structural information is available (Figure 6), suggesting that P7 will disrupt binding to these proteins as well.

### **Second generation peptide specificity and cellular target engagement**

The two tightest binding second generation peptides, P1 and P7, were next synthesized with FAM and 9R additions for use in cell assays. The tagged proteins were first tested for their ability to bind Cdc42. As the specificity of the interaction of these peptides is likely to be paramount for any future therapeutic, a survey of the binding affinities of these peptides across a wider panel of small GTPases was also undertaken. The panel of small G proteins tested included both Cdc42·GDP and Cdc42·GMPPNP along with the classic Rho-family exemplars, Rac1 and RhoA. We also included members of the Ras family: K-Ras and RalA as examples of more diverse small G proteins. Binding of tagged C1, P1 and P7 with the selected small G proteins was assessed using FP. The results are shown in a radar plot in Figure 7 and are tabulated in Table 2. All three peptides have relatively weak affinity for K-Ras and RalA as expected. The data demonstrate that overall P7 has higher specificity than C1 or P1, showing considerably tighter binding to Cdc42 and Rac1 than other small-GTPases. P1 and C1 have more similar specificity profiles and bind RhoA with comparable affinity to Cdc42 and K-Ras to a

### *Inhibition of Ras-Cdc42 signalling by a cyclic peptide*

lesser extent. All three peptides however show only marginally better binding to Cdc42·GMPPNP than Cdc42·GDP.

Cellular entry of these second generation peptides was demonstrated by confocal microscopy using A549 cells. The A549 cell line is a human lung epithelial cell line, which is homozygous for K-Ras G12S. As such it is a good representative of the type of cells in which these peptides would need to be active therapeutically. The images in Figure 8A show representative examples of cells treated with C1, P1 and P7 at varying time points after addition. The peptides concentrate at the periphery of cells in vesicular structures at 1 hour time points but are able to access the interior of the cell and appears to be distributed in the cytosol rather than concentrated, potentially in endosomes, after 3-6 h, in contrast to the previous studies using MEFs.

The efficacy of the peptides in inhibiting the interaction of Cdc42 with its effector proteins was next tested using GST-effector domain pulldown inhibition assays in cell lysate. Increasing concentrations of unconjugated C1, P1 and P7 were introduced into A549 cell lysate and the ability of Cdc42 to interact with the effector binding domains assessed. The data in Figure 8B (upper panels) show the inhibition of the endogenous Cdc42 interaction with immobilised GST-WASP GBD by peptides C1, P1 and P7 (experiments were also performed with ACK GBD showing similar inhibition, data not shown). These data suggest that the binding of the peptides to Cdc42 is sufficiently stringent to inhibit Cdc42-effector interactions amongst the myriad of proteins in cell lysate.

These experiments were repeated with FAM-9R conjugated peptides to determine if these additions affected targeting of Cdc42 in cell lysates. These data were quantified and are shown, together with the data from the unconjugated peptides, in the

graph in Figure 8B (lower panel). The data shows that the FAM-9R conjugated peptides inhibited the Cdc42-WASP interaction but a considerably higher concentration was needed to achieve this than with the unconjugated peptides. The IC<sub>50</sub>s calculated from these data suggest that, in fact, the addition of FAM-9R to the peptides results in a >10X decrease in efficacy in cell lysates. For example IC<sub>50</sub> C1 is 190nM ± 62 nM but for FAM-C1-9R is 2200 ± 740 nM. For P7 the effect is even greater with the IC<sub>50</sub> P7 calculated as 1.2 ± 0.28 nM but for FAM-P7-9R being 65 ± 12 nM. Importantly these data suggest that any cellular effects seen with the peptides will be greatly enhanced when using an alternative delivery system and/or without the reporter group.

Peptide binding to Cdc42 *in vitro* was further demonstrated using cellular thermal shift assays (CETSAs)(40). These assays monitor protein stability during thermal denaturation in cells or in lysate, in the presence of potential binding partners or inhibitors. Changes in thermal stability are taken as an indication of protein engagement by the peptides. Cdc42 levels were monitored under appropriate conditions in A549 cell lysates, with the addition of increasing concentrations of peptide P7 and the results are shown in Figure 8C. Cdc42 in lysates is destabilized in the presence of P7, indicating target engagement by the peptide. These experiments were repeated in A549 cells with peptide P7 added in to the cell growth media and allowed to enter cells for 3.5 hours (Figure 8D). The results show a similar destabilization pattern of Cdc42 when the cells are exposed to peptide. Interestingly, at higher peptide concentrations (3-6 μM), which are toxic to cells, a rise in Cdc42 levels was noticed which then similarly decreased with concentration, potentially implying a different transport mechanism takes over that does not allow similar levels of target engagement.

#### *Inhibition of Ras-Cdc42 signalling by a cyclic peptide*

##### **The second generation peptides significantly inhibit transformation phenotypes in A549 cells**

As the peptides were able to enter cells and engage with Cdc42, the effects of the peptides on cellular properties associated with transformation were assessed. Firstly proliferation was measured. The longevity of either the peptide sequences themselves or the disulphide bond was unknown in cells, however as the experiments in MEFs (Figure 2D) showed signalling restoration with time, the peptides were redosed at 24 hours, and 48 hours was used as an upper time limit in proliferation experiments. After 48 hours incubation, cells treated with a 1 μM dose of the peptides showed significantly lower proliferation levels compared to the 9R control, as shown in Figure 9A. The most pronounced effect was seen for P1, while C1 and P7 show similar but slightly reduced potency. At 5μM doses, greater inhibition of proliferation is seen, with a similar pattern of peptide efficacy. Overall, for all three peptides, C1, P1 and P7, statistically there is a significant linear trend both with increasing dose and increasing time of incubation (using general linear models in R, data not shown), while this is not seen for 9R, further demonstrating biological activity for these peptides.

Cdc42 and other Rho family small G-proteins are traditionally associated with cytoskeletal rearrangements, which govern cell motility (41). High migration and motility are also associated with aggressive oncogenic phenotypes and inhibition of this would therefore be highly desirable. It was notable from the proliferation assays that the 9R CPP alone begins to have a significant effect on cell proliferation at concentrations above 5 μM and as such peptides were only dosed at 1 μM in subsequent experiments. Peptides were first assessed in Boyden chamber assays monitoring invasion and migration towards higher serum concentrations and the results are shown in Figure 9B. Potent effects for the peptides dosed at 1 μM were

observed. The data also show significant inhibition of invasion and migration by the 9R control (~65%), however the peptide-9R conjugates showed greater inhibitory effects, in particular P1 and P7 which reduce invasion and migration by around 90% and 85% respectively.

Next, wound healing assays were used to monitor co-ordinated cell motility and proliferation. A549 cells were treated with 1  $\mu$ M FAM-peptides-9R and monitored for 48 h. Representative images and data plots are shown in Figure 9C. All peptides showed significant inhibitory effects on wound closure; in the case of P1 and P7, the scratch area did not close within the duration of the assay. In contrast to the Boyden chamber assays no inhibitory effect was noted for 9R alone.

Taken together these data suggest that the high affinity Cdc42 binding peptides developed here have the hallmarks of early lead molecules for therapeutic intervention in Ras-driven cancers.

## Discussion

The isolation and maturation of a peptide, C1, capable of binding Cdc42 with mid nM affinity, from the naïve libraries used in the original display experiments described here, validates CIS display as a robust technique for isolating small G protein binding peptides. Molecular display methods all have to rely on the chance sampling of library members to some extent, as seldom, even with larger libraries, can all sequence space be covered for peptides beyond 10 residues in length. However, as a wholly acellular technology, CIS display, with larger, stable libraries, is likely to sample greater sequence space and thus allow the identification of tighter binding peptides. Subsequent maturation of C1 increased both the specificity and affinity of this peptide further, with the best second generation binders containing 2-4 mutations at 6 positions and possessing ~17-fold increased binding to their primary target, Cdc42·GTP. Whilst the use of a randomly doped

## *Inhibition of Ras-Cdc42 signalling by a cyclic peptide*

maturation library has identified 6 positions as being important for the improvement of binding efficiency, display of this library may still not have allowed sampling of all the most beneficial combinations of mutant residues. Further affinity maturation may be possible by using mutagenesis directed to these 6 positions particularly if harnessed with competitive regimes of selection. Alternatively, a rational design approach and the incorporation of unnatural amino acids may offer further scope for improved affinities.

Closer investigation of C1 and its derivatives has demonstrated that the specificity for active Cdc42 was not as high as initially indicated (see Figure 1B vs. Figure 7) with the peptides binding closely related small GTPases. Binding to Cdc42 is also insensitive to the nucleotide state, thus the peptides may also interfere with Cdc42 interactions when inactive. Peptide maturation has however resulted in tighter Cdc42 binding and also modulation of Rho family specificity. P7 in particular shows improved targeting of Rac1 and Cdc42 over other Rho family proteins and K-Ras.

In general, tighter binding to a target does correlate with increased specificity. This holds true for general off-target binding events, however does not necessarily follow for proteins very closely related to the target itself. For a potential therapeutic designed to target small G proteins, there are many very closely related proteins that the molecule could encounter.

The data-driven model we generated of the Cdc42-P7 complex suggests some hypotheses as to how residue replacements in the second generation peptides have influenced binding. The key replacements at the Arg8 and Asp10 positions may allow a salt bridge to form between Asp10 and Lys166<sup>Cdc42</sup>, while Arg8 lies close to Tyr23 in Cdc42 helix  $\alpha$ 1 and could form a polar interaction here. The replacement of His8 and Gln10 in C1 and P1 for charged residues in P7 therefore increases the affinity of P7, by imparting the

ability to form the ionic interaction involving Asp10<sup>P7</sup> and Arg8<sup>P7</sup>.

The most marked difference between P7 and C1/P1 is the reduced binding to RhoA by P7, which is likely due to Arg8 and Asp10. Tyr23<sup>Cdc42</sup>, which, in the model, is close to Arg8 in P7, is replaced by Phe in RhoA, which would remove any polar interaction between these sidechains. Lys166<sup>Cdc42</sup>, which forms a salt bridge with Asp10<sup>P7</sup> in the model, is still present in RhoA, but Met45<sup>Cdc42</sup>, which is also close to Asp10, is replaced by Glu in RhoA. This could potentially destabilize the binding of Asp10 at this site. These interactions and substitutions between Rho family members potentially explain the specificity of P7 for Cdc42 and Rac1 and could be used to guide fine-tuning of specificity, although detailed structural data on the Cdc42- P7 complex would be necessary to underpin any rational design campaign.

Our structure of P7 also explains some important structural features of the peptide. Our binding data indicate the importance of the cyclized nature of the peptides in engaging their target. In fact cyclizing libraries were deliberately utilized in the initial stages of this project to exploit the utility of cyclic peptides as therapeutics. As it is difficult to introduce stable macrocycle linkages into a biological display strategy, the non-variant incorporation of cysteine residues was exploited in these libraries to allow disulphide formation and provide a useful platform to screen cyclic peptides. However the potential instability of a disulphide bond in cells was always acknowledged.

Disulphide bonds are regulated inside the cell by an array of enzymes and redox molecules such as thioredoxin, glutathione and NADPH that increase the naturally slow turnover of disulphides (42). The major redox couples that govern cellular redox potential are not necessarily in equilibrium with each other and indeed the equilibria vary

#### *Inhibition of Ras-Cdc42 signalling by a cyclic peptide*

between intracellular compartments, generally being defined by the reduced/oxidised glutathione ratio (42). Endosomes have an oxidising potential while the cytosol is mainly reducing (43), and it is thought that a disulphide could survive intact through endocytosis (44) but upon endosomal escape the peptide enters a reducing environment. How long the disulphide would last under these conditions is not easy to define as data are confounded by uptake and release rates from endosomes (45). Available data suggest that a disulphide bond in cyclized peptides may last in the extracellular environment but could start to come under attack from the point of interaction with a cell, however they are likely to pass through the endocytic pathway in an oxidised form. Upon release into the cytosol, disulphide bridged cyclic peptides should be quickly reduced, diminishing their binding affinity and proteolytic stability. Peptides however will be taken up and released into the cell as a gradual process; meaning release into the cytosol will be continual.

In light of the possible instability of our lead peptides in cells, we have trialled various strategies to produce stable cyclized versions of these peptides. The replacement of the disulphide with a lanthionine bridge by alkali-catalysed desulphurization (46) rendered this linkage non-labile in reducing environments and the resulting peptides retained the same binding affinity as disulphide linked forms *in vitro* and in CETSA lysate experiments (data not shown), suggesting that, with the appropriate chemistry, stable cyclized versions of these peptides can be successfully engineered if necessary. However, the biological data presented here was all obtained using disulphide linked peptides. Our data suggest that these disulphide linked peptides are actually relatively stable in a cellular environment, with biological effects seen up to 24 hours after exposure to peptides. The structure of the P7 peptide reveals that it is remarkably rigid and it is possible that the highly compact nature of P7

protects the disulphide bond to some extent, so that it is less labile in a cellular environment than a more flexible peptide might be. The rigid P7 structure contributes to its high affinity, since the binding loop containing Arg8 and Asp10 is pre-formed and there will be no entropic penalty when it binds to the G protein. The peptide-binding site, determined by experimental chemical shift mapping, is within a pocket formed by the  $\beta$ 2 strand and helices  $\alpha$ 1 and  $\alpha$ 5 in Cdc42. This site is away from the nucleotide binding site and the nucleotide-sensitive switch regions of Cdc42, which explains the ability of P7 to bind Cdc42 without nucleotide specificity. Nevertheless, peptide P7 can still compete with ACK for binding to Cdc42 (Figure 3) and is presumably an orthosteric inhibitor, given the overlap between the ACK and P7 binding sites. However, Cdc42 is, like all small GTPases, an allosteric protein (reviewed in (47)), and it is possible that P7 will disrupt binding of other proteins, such as GDIs and exchange factors, that do not directly engage with the P7 binding pocket.

The model of the Cdc42-P7 complex may also explain the observation that Cdc42 engagement by P7 leads to destabilization of the small G protein (Figure 8C and D). This was potentially unexpected, given that the binding of the CRIB effectors is likely to stabilize both binding partners as two disordered regions coalesce into a more rigid complex (48). Other systems using CETSA have reported stabilization, destabilization and no-change with target engagement and the effect appears difficult to predict (49,50). However the distinct binding mode of P7, interacting with regions that are already structured in the free Cdc42 would not necessarily stabilize the protein and could potentially inhibit interaction with binding partners that confer thermal stability.

The addition of a CPP motif allowed the peptides access to the cell interior in both MEF and A549 cells. The general mechanism of CPP entry has

#### *Inhibition of Ras-Cdc42 signalling by a cyclic peptide*

been a subject of some debate but appears most likely to be through endosomal uptake and escape (51). Certainly this seems to be the case with the peptides described here. The kinetics of cellular distribution appear to be different in MEFs and A549s, however in both cell types the effects observed suggest sufficient peptide delivery to the target to obtain measurable biological effects.

Pulldown inhibition in lysates has demonstrated that the peptides are specific and soluble enough among the cell contents to bind and inhibit Cdc42-effector interactions, but, interestingly, the addition of N-terminal FAM and C-terminal 9R considerably reduce the potency of Cdc42 interaction inhibition. The most likely reasons for this approximately 10-50-fold reduction in potency are that the 9R motif binds non-specifically to other moieties or causes aggregation in the lysate. These results suggest that the cellular potency of the peptides is reduced by this CPP motif, an effect that is likely to be general to peptides using a 9R CPP. No therapeutics have made it to clinical trials using such a motif and, aside from the toxicity issues which are confirmed in Figure 2C, this reduction in target specificity could be a contributory reason in some cases. An alternative delivery system therefore should dramatically improve potency in this case. Methods to improve delivery could either employ a cleavable linker or another cell penetration strategy.

The early promise of C1 in decreasing signalling to STAT3 and ERK1/2 in MEFs has been consolidated by potent second generation peptide effects on proliferation and especially migration in the more aggressive A549 cell line. The fact that these peptides were selected to target the Rho-family small-GTPases, which are known to control cytoskeletal structure and migration, makes it encouraging that the most potent effects of the matured peptides are on cell motility. Data presented here have demonstrated effective target

engagement in the cellular environment, however it is uncertain how important inhibition of off-target small-GTPases is to overall peptide efficacy. P1 shows more potency than P7 in Boyden chamber and proliferation assays despite having a lower affinity for Cdc42. P1 however has relatively high affinity for RhoA and it may be that inhibition of RhoA, or indeed another related Rho GTPase, is important for these effects. P7 performs best in wound healing assays, where, presumably, high affinity for Cdc42 is most efficacious. Our data, therefore, suggest that simultaneous targeting of several Rho family GTPases could result in improved anti-oncogenic effects; indeed arguments for true polypharmacology are presently redefining drug discovery paradigms (52). This opens up interesting future studies into how inhibition by different peptide derivatives from C1 could tune various signalling pathways and phenotypic effects.

The effect we see on ERK1/2 signalling is an interesting example of the type of effects we were hoping to see in these peptides. Traditionally ERK1/2 phosphorylation is monitored as a readout for Ras signalling. We see down regulation of pERK1/2. However in this case we assume that this is due to inhibition of the Cdc42-PAK complex. PAK is another CRIB effector of Cdc42 (and indeed of Rac1), which is known to be involved in regulation of ERK activity as it regulates phosphorylation of both Raf and MEK, contributing to activation of the Raf-MEK-ERK pathway (53,54). Thus the peptides appear to inhibit the interaction of Cdc42 (and possibly other Rho-family GTPases) with multiple effectors due to the similarity in the effector engagement sites and act as blockades of Cdc42 signalling. The similarity in the CRIB-effector interfaces and their overlap with the P7 binding site (Figure 6) provide a rational explanation for the ability of P7 to inhibit multiple effector pathways.

#### *Inhibition of Ras-Cdc42 signalling by a cyclic peptide*

In summary, the peptides isolated in this study show promise as inhibitors of oncogenic phenotypes in Ras-driven cancers, a hugely important cohort of cancers that have proved difficult to treat to date. Their activity is dependent on their cyclic nature and while they appear to contain a relatively stable disulphide bond, which confers activity in cells for several hours, introduction of a non-labile cyclization was also possible without compromising activity. Other strategies to increase stability of the peptides using unnatural bonds and residues are currently under investigation. Utilization of a 9R CPP motif for experimental purposes was successful but a 9R control peptide did show significant toxic effects on cells above a threshold concentration. More importantly the 9R CPP, when conjugated to the peptides, reduced target engagement by ~10-50-fold in cell lysate. Alternative peptide entry strategies are also currently under investigation and should dramatically improve efficacy of these peptides *in vivo*. Slight changes in the C1 peptide sequence were also shown to modulate specificity to small GTPases and change phenotypic effects suggesting that the target selection of these peptides can be adapted. A degree of polypharmacology is also likely to be desirable in future anti-cancer therapeutics and tuning alternative-target binding should improve therapeutic properties further.

The peptides we describe here are examples of peptide macrocycle technology applied to the highly intractable target class of small G proteins and represent a promising new modality for future therapeutics. Our data also adds to the growing literature demonstrating that peptides are establishing their place in the biologics arm of drug discovery. Importantly here we create early lead therapeutic biologics for one of the most urgent clinical needs in cancer presented today.

## Experimental Procedures

### Protein preparation

Target proteins were expressed in pGEX-2T (GE Healthcare) as GST fusion proteins. Constructs expressing the ACK and WASP GBDs, Cdc42  $\Delta$ 7 Q61L, Cdc42  $\Delta$ 7, Rac1  $\Delta$ 7 Q61L, RhoA  $\Delta$ 12 Q63L, RalA  $\Delta$ 21 Q72L and RalB  $\Delta$ 21 Q72L have been previously described (55-57). Human K-Ras 4B (residues 1-169) was amplified by PCR and cloned into pGEX-6P (GE Healthcare) using *Bam*HI and *Eco*RI sites that had been incorporated into the PCR primers. A Q61L mutation was introduced using QuikChange Lightning mutagenesis (Agilent), following manufacturer's instructions. Recombinant proteins were expressed in *E. coli*, affinity purified on glutathione agarose resin (Sigma-Aldrich) and cleaved (except for GST ACK/WASP) from GST using thrombin (Novagen) or C3 protease. Cleaved proteins were purified by gel filtration (S75 16/60, GE Healthcare), while GST ACK/WASP were purified by ion exchange as described previously (18,37). Nucleotide exchange reactions were performed for small G proteins to add the non-hydrolysable GTP analogue, GMPPNP, or tritiated GTP as described previously (18). Cdc42 was biotinylated for use in CIS display. EZ-link Sulfo-NHS-biotin (ThermoFisher) was incubated for 30 min at room temperature with Cdc42 at a molar ratio of 20:1. Reactions were performed in PBS according to manufacturer's instructions and the protein recovered from the reaction mix using PD10 desalting columns (GE Healthcare).

### CIS display

Three naïve library populations were created by mixing 10 random peptide encoding libraries generated from oligonucleotide primers purchased from Ella Biotech GMBH. The variant regions of these primers were built from DNA trimers designed to give equal amino acid frequencies (with the exclusion of cysteine) and optimized for expression in *E. coli*. Linear libraries comprised varying lengths of contiguous random amino

### *Inhibition of Ras-Cdc42 signalling by a cyclic peptide*

acids, whilst cyclic libraries followed a sequence pattern of  $X_3CX_NCX_3$  where X denotes random amino acid representation (excluding Cys) and N was defined by the library length. The C1 maturation library conserved the cysteine residues for cyclic linkage but introduced biased mutagenesis at all other nucleotide positions, with 79% parental conservation and 7% incorporation of each non-parental nucleotide. CIS display construct synthesis and biopanning reactions were performed as previously described (19). For heat elutions DNA was eluted from streptavidin beads by heating to 75 °C for 10 min, whereas in competitive elutions, beads were incubated for 1 h in 100  $\mu$ L PBS + 2% BSA + 50  $\mu$ M ACK GBD and the supernatant recovered. Four rounds of biopanning were performed for each selection and for the maturation campaign, before library analysis by next generation sequencing using the MiSeq Desktop Sequencer (Illumina).

### Phage ELISAs

Library DNA from selections and pHEN-1 phagemid vector were digested with *Nco*I and *Not*I, ligated together and transformed into TG1 *E. coli* cells (Lucigen). Transformants were picked at random and 30  $\mu$ L of overnight culture derived from individual colonies was used to seed cultures in 300  $\mu$ L 2TY, 2% glucose, 100  $\mu$ g/mL ampicillin, which were incubated at 37 °C with shaking to O.D.<sub>600</sub> = 0.3. 10<sup>8</sup> pfu M13K07 helper phage in culture medium were added to each well and the cultures incubated for 1 h at 37 °C without shaking. Cells were centrifuged, the supernatant discarded and bacteria resuspended in 400  $\mu$ L 2TY, 100  $\mu$ g/mL ampicillin, 25  $\mu$ g/mL kanamycin per well and incubated overnight at 37 °C with shaking to allow phage expression. The recombinant phage were recovered in the supernatant after centrifugation for screening.

NUNC Maxisorp plates were coated overnight with streptavidin (Pierce) at 250 ng per well for assays using biotinylated Cdc42. Assay plates for

specificity tests were coated directly with 500 ng per well, recombinant small GTPases or bovine serum albumin (BSA). Wells were washed in PBS and blocked in 1% BSA in PBS for 2 h at 20 °C. The streptavidin plates were then incubated with biotinylated Cdc42·GMPPNP (100 ng per well for 30 min) and the wells subsequently washed in PBS.

In parallel the phage were blocked in PBS containing 1% BSA for 2 h then added to target coated ELISA plate and shaken for 1-2 h at room temperature. Plates were washed (3 X PBS-Tween 0.1%, 2 X PBS) to remove unbound phage and then incubated with anti M13/HRP antibody conjugate (B62-FE2, Abcam: 1/5000 dilution in PBS containing 2% BSA). Plates were washed as before and TMB (eBioscience) (50 µL per well) added. Wells were quenched with 50 µL 0.5M H<sub>2</sub>SO<sub>4</sub> after blue colouration was visible and A<sub>450</sub> measured using a Multiskan EX (Thermo Scientific). DNA from phage clones was amplified by PCR and sequenced (Beckman Coulter).

### Peptide synthesis

Peptides with an amidated C-terminus were synthesized on a 10µmol scale by standard Fmoc solid-phase chemistry on an automated peptide synthesizer (MultiPep RS, Intavis, Germany). Following the final Fmoc deprotection, the peptide N-terminus was acetylated (4% acetic anhydride, 16% N-methylpyrrolidone (NMP) in dimethylfluoride (DMF) for 1 h), biotinylated (12 equivalents biotin, 12 equivalents Hexafluorophosphate Benzotriazole Tetramethyl Uronium (HBTU), 5% N-methylmorpholine (NMM) in DMF overnight) or 5(6)-FAM labelled (5 equivalents 5(6)-FAM, 5 equivalents HBTU, 10 equivalents NMM in DMF overnight). Resin was extensively washed with dichloromethane and methanol, and dried overnight. After deprotection and cleavage from the resin (TentaGel, Intavis, Germany) with 5% water, 5% phenol, 5% thioanisole, 2.5% ethanedithiol in trifluoroacetic

### *Inhibition of Ras-Cdc42 signalling by a cyclic peptide*

acid (TFA) for 3 h, the peptides were precipitated in diethylether at -20 °C. The crude peptides were purified by reverse-phase HPLC (Shimadzu) using a C<sub>18</sub> column (50 x 250mm, SunFire, Waters) and a linear gradient elution 20-50% acetonitrile in 0.1% Trifluoroacetic acid (TFA). The molecular masses were determined by MALDI-TOF-TOF mass spectrometer (AXIMA Assurance, Shimadzu). Nona-arginine linked peptides were purchased from Cambridge Research Biochemicals.

### Scintillation proximity assays (SPAs)

30 nM GST wt-ACK GBD was immobilised on Protein A SPA fluoromicrospheres (Perkin Elmer) *via* an anti-GST antibody (Sigma-Aldrich). 30nM [3H]GTP·Cdc42 was added and the effect of competition measured by measuring the signal in the presence of increasing concentrations of the peptide under test. Scintillation counts were measured at each concentration and fitted to the appropriate binding isotherm as described previously (58).

### Fluorescence polarization

Fluorescence polarization (FP) experiments were measured on a BMG Labtech Pherastar fluorimeter at 298 K with excitation 485 nm and emission 520 nm. Solutions were made up in black flat-bottom 384 well plates (Corning) to a final volume of 30 µL. Anisotropy was calculated from polarization measurements in MARS analysis software and data fitted to binding isotherms in R(59). Direct binding data was fitted using equation 1, while competition data was fitted to a previously described equation (58).

$$y = S_{min} + (S_{max} - S_{min}) \times \frac{C}{K_d + C} + (Max - NSB) \times C \quad \text{Eq 1}$$

Where y equals anisotropy; S<sub>max</sub> equals the maximum binding signal; S<sub>min</sub>, the minimum binding signal; C, the target concentration and

NSB, the non-specific binding component. For direct binding assays a concentration range of small GTPase was added to FAM-labelled peptides (60 nM) while in competition assays dilutions of unlabelled C1 peptide was added to 60 nM FAM-C1 and 500 nM Cdc42·GMPPNP.

### NMR Spectroscopy and Structure Calculations.

<sup>15</sup>N HSQC Experiments were recorded on a Bruker DRX500 at 298 K in 50 mM Tris-HCl pH 7.5, 1 mM MgCl<sub>2</sub>, 5 mM DTT, 150mM NaCl, 10% D<sub>2</sub>O. For the titration experiments 0.25, 0.5, 1 and 1.25 equivalents of peptide were added to <sup>15</sup>N-labelled Cdc42 and spectra were recorded after each peptide addition. Overall chemical shift perturbations,  $\delta$ , were calculated using equation 2;

$$\delta = \sqrt{\delta_{iH}^2 + (0.15\delta_{iN})^2}$$

Eq 2

where  $\delta^1H$  and  $\delta^{15}N$  are the chemical shift changes for the <sup>1</sup>H and <sup>15</sup>N dimensions, respectively.

2D NOESY (250 msec mixing time), TOCSY (65 msec mixing) and DQF-COSY experiments were recorded on peptide P7 on a Bruker AV800 at 298 K in 50mM sodium phosphate, pH 7, 10% D<sub>2</sub>O.

All NMR data were processed using the *AZARA* package (Wayne Boucher, University of Cambridge) and analysed using CCPN *ANALYSIS* (60). Peptide structures were calculated using *ARIA* 1.2 (61) interfaced to *CNS* (62) where the ambiguity of the restraints was decreased during eight iterations. Cdc42 residues whose backbone amides had shifted by more than 0.043 (the average shift change) and which were more than 40% solvent exposed in either of two structures (according to *NACCESS* (63)) were used as active residues in *HADDOCK* (38,39). *HADDOCK* was also run including only residues whose backbone amides had shifted by more than 0.090 (the average shift change plus 1 standard deviation). In all cases, residues whose peaks had shifted too far to be reliably assigned were included as active residues. The Cdc42 structures used were those

### *Inhibition of Ras-Cdc42 signalling by a cyclic peptide*

from complexes with Par6 (PDB code 1nf3) or IRSp53 (PDB code 4js0), where the effector was removed in each case. *HADDOCK* was run twice for each set of active residues, once with each of these structures as a starting point. In all *HADDOCK* runs the top cluster showed the peptide binding in the same orientation on the same surface of Cdc42. The active Cdc42 residues were as follows (after filtering for solvent exposure): shifted by more than average + 1 SD, 25, 46, 49, 164; shifted by between average and average +1 SD, 3, 12, 26, 62, 76, 116, 153, 167, 177, 178; shifted too far for unambiguous assignment to be possible, 24, 30, 43, 48, 52, 160, 162, 166. Passive residues were defined automatically by *HADDOCK*. Active residues for the peptide were defined as 8 and 10, with all other peptide residues being passive.

### Immunoblotting

Lysates were taken from 2 X 6 cm dishes in 100  $\mu$ L lysis buffer (50 mM Tris-HCl pH 7.5, 150 mM NaCl, 1 mM EDTA, 1 mM sodium orthovanadate, 1 mM  $\beta$ -glycerophosphate disodium salt hydrate, 1X protease inhibitor cocktail (Mammalian, Sigma Aldrich), 1% Triton X-100) and centrifuged at 17,000 g for 20 min. Cell samples were resolved by SDS-PAGE and immunoblotted using the following primary antibodies:  $\alpha$ -Stat3 (F-2) sc-1019,  $\alpha$ -Stat3 (Y705) sc-7993 (Santa Cruz Biotechnology),  $\alpha$ -GAPDH-HRP ab9482 (Abcam),  $\alpha$ -Erk1/2 9107S,  $\alpha$ -pErk1/2 4376S (Cell Signaling Technology).

### Cellular Thermal Shift Assays (CETSA)

For CETSA lysate experiments A549 cells were trypsinized, washed in PBS and resuspended in lysis buffer (50 mM Tris-HCl pH 8.0, 50 mM NaCl, 5 mM MgCl<sub>2</sub>, 1X protease inhibitor cocktail (Mammalian, Sigma Aldrich)) at 60,000 cells/50  $\mu$ L. Cells were lysed by three freeze-thaw cycles in liquid nitrogen and centrifuged. Supernatant was divided into 50  $\mu$ L aliquots, which were exposed to varying concentrations of peptide or

### *Inhibition of Ras-Cdc42 signalling by a cyclic peptide*

temperatures. Cell lysates were first heated over a wide range of temperatures to determine the melting temperature of the protein under investigation. Samples were heated for 3 min in a Veriti 96-well thermal cycler (Applied Biosystems), then cooled for 3 min and centrifuged. Supernatants were analysed by Western blot. Lysates were then tested over a narrower range of temperatures below the melting temperature, +/- a fixed concentration of the peptide under test and a temperature was identified where a peptide effect was apparent; this temperature was set as the experimental temperature. Finally lysates were tested at the experimental temperature with a range of peptide concentrations. For whole cell experiments 600,000 A549 cells were seeded in 12-well culture plates and incubated for 3.5 h. Cells were trypsinized, collected and washed in PBS. Samples were heated for 3 min as above, 30  $\mu$ L lysis buffer added (25 mM Tris-HCl pH 7.5, 5 mM  $\beta$ -glycerophosphate, 2 mM DTT, 0.1 mM sodium vanadate, 10 mM  $MgCl_2$ ), then subjected to two freeze-thaw cycles before. The supernatant was analysed by Western blot. An experimental temperature was determined as above. Cells were then plated and incubated with a range of peptide concentrations for 3.5 h and analysed as above.

#### **GST pulldown assays**

Glutathione sepharose (GE Healthcare) in PBS was incubated for 15 min at 4 °C with GST-WASP and then washed three times in PBS, 0.1% Tween. 25  $\mu$ g GST-WASP attached to beads was incubated with 100  $\mu$ L A549 lysate for 45 min in the presence of varying peptide concentrations. Beads were washed twice in PBS, 0.1 % Tween. Samples were resolved by SDS-PAGE and immunoblotted using an anti-Cdc42 antibody (610928, BD Biosciences). Western blots were quantified using Image J and data fitted to equation 3 to calculate IC50 values.

$$\% \text{ Signal} = \frac{100 - 100 / (1 + IC50 / \text{concentration})}{100} \quad \text{Eq 3}$$

#### **Proliferation assays**

100  $\mu$ L A549 cells were seeded in 96-well culture plates (CellStar) at 50,000 cells/mL and allowed to settle overnight. Peptides were dosed in 4  $\mu$ L PBS every 24 h. After 48 h 10  $\mu$ L MTT (Invitrogen, 5 mg/mL in PBS) was added and the plates incubated for 2-3 h. Medium was removed and 100  $\mu$ L DMSO added to solubilize the contents. After 4 h the  $A_{570}$  absorbance was measured of each well in a SoftMax Pro 5 (Molecular Devices).

#### **Boyden chamber assays**

Upper chambers of Boyden chambers (BRAND) were seeded with 50,000 A549 cells in 100  $\mu$ L RPMI, 0.1% FCS with 1  $\mu$ M peptide doses. The bottom chamber was filled with RPMI, 10% FCS and the plates incubated for 5.5 h at 37 °C. Cells and media were removed from the top chamber using cotton buds and the media in the bottom well replaced with trypsin and incubated for 10 min at 37 °C. The cells were removed, centrifuged and the cell pellets resuspended in 20  $\mu$ L PBS. Cell suspensions were counted on the Countess automated cell counter (Invitrogen) and data analysed and plotted in R.

#### **Wound Healing Assays**

3 well microdishes (Ibidi) were seeded with 20,000 A549 cells in 100  $\mu$ L RPMI/well and allowed to settle overnight. Wells were dosed with 1  $\mu$ M peptide and incubated for 3 h. 0.5 mL medium with 1  $\mu$ M peptide was added to the outside of the dishes and the inserts removed. Images were taken at various timepoints using an EVOS fl digital inverted microscope (AMG) at 4X magnification. Images were cropped to 680 by 512 pixels (width approximately 1 mm) and scratch area analysed using the MiToBo package in Fiji (64,65). Data were processed in R.

#### **Confocal microscopy**

Cells were seeded at 50,000/mL in micro-insert  $\mu$ -dishes (Ibidi) and incubated overnight. Peptides were added in fresh medium and cells incubated

for respective timepoints. Cells were washed 4 X with PBS and imaged in imaging medium (H0887, Sigma) in a stage top heated chamber (Okolabs) at 37 °C. Confocal images were acquired on an inverted Ti-E microscope (Nikon) with a spinning-disk (X-light Nikpow, Crest), 250 µm Lunencor Sprecra X LED illumination and a piezo driven Z stage controller (NanoScanZ) using a 100 X 1.40,

#### *Inhibition of Ras-Cdc42 signalling by a cyclic peptide*

oil objective lens (Plan Apo VC, Nikon). Images were collected with an EMCDD camera (Evolve Delta, Photometrics) with Metamorph software (version 7.8.2.0). 5(6) FAM samples were visualized using a 470/40 excitation and 525/50 emission filters and images processed in Fiji (64,65).

**Acknowledgements:** We are extremely grateful to Dr Chris Ullman and Dr Kevin Matthews for their belief in peptide therapeutics and support of this project. We thank Dr Cathy Wilson for expert assistance and advice in producing MEFs for this work. We are also indebted to Dr Jenny Gallop and Dr Jonathan Gadsby for help in performing confocal experiments. This research was supported by an MRC CASE Studentship (MR/K017101/1) to DO and RNC, a BBSRC DTP iCASE Studentship (BB/M011194/1) to DO and JR and a short-term Glover Research Fund Fellowship to GJNT.

**Conflict of interest:** The authors declare that they have no conflicts of interest with the contents of this article.

#### **References**

1. Li, S., Balmain, A., and Counter, C. M. (2018) A model for RAS mutation patterns in cancers: finding the sweet spot. *Nat. Rev. Cancer* **18**, 767-777
2. Ostrem, J. M., and Shokat, K. M. (2016) Direct small-molecule inhibitors of KRAS: from structural insights to mechanism-based design. *Nat Rev Drug Discov* **15**, 771-785
3. Spencer-Smith, R., and O'Bryan, J. P. (2017) Direct inhibition of RAS: Quest for the Holy Grail? *Semin. Cancer Biol.* **54**, 138-148
4. Mott, H. R., and Owen, D. (2018) Bioblockades join the assault on small G protein signalling. *Semin. Cancer Biol.* **54**, 149-161
5. Ridley, A. J. (2015) Rho GTPase signalling in cell migration. *Curr. Opin. Cell Biol.* **36**, 103-112
6. Arias-Romero, L. E., and Chernoff, J. (2013) Targeting Cdc42 in cancer. *Expert Opin. Ther. Targets* **17**, 1263-1273
7. Stengel, K. R., and Zheng, Y. (2012) Essential Role of Cdc42 in Ras-Induced Transformation Revealed by Gene Targeting. *PLoS One* **7**, e37317
8. Fritz, G., Brchetti, C., Bahlmann, F., Schmidt, M., and Kaina, B. (2002) Rho GTPases in human breast tumours: expression and mutation analyses and correlation with clinical parameters. *Br. J. Cancer* **87**, 635-644
9. Tucci, M. G., Lucarini, G., Brancorsini, D., Zizzi, A., Pugnali, A., Giacchetti, A., Ricotti, G., and Biagini, G. (2007) Involvement of E-cadherin, beta-catenin, Cdc42 and CXCR4 in the progression and prognosis of cutaneous melanoma. *Br. J. Dermatol.* **157**, 1212-1216

*Inhibition of Ras-Cdc42 signalling by a cyclic peptide*

10. Liu, Y., Wang, Y., Zhang, Y., Miao, Y., Zhao, Y., Zhang, P. X., Jiang, G. Y., Zhang, J. Y., Han, Y., Lin, X. Y., Yang, L. H., Li, Q. C., Zhao, C., and Wang, E. H. (2009) Abnormal expression of p120-catenin, E-cadherin, and small GTPases is significantly associated with malignant phenotype of human lung cancer. *Lung Cancer* **63**, 375-382
11. Lin, R., Cerione, R. A., and Manor, D. (1999) Specific contributions of the small GTPases Rho, Rac, and Cdc42 to Dbl transformation. *J. Biol. Chem.* **274**, 23633-23641
12. Hamann, M. J., Lubking, C. M., Luchini, D. N., and Billadeau, D. D. (2007) Asef2 functions as a Cdc42 exchange factor and is stimulated by the release of an autoinhibitory module from a concealed C-terminal activation element. *Mol. Cell. Biol.* **27**, 1380-1393
13. Durkin, M. E., Yuan, B. Z., Zhou, X., Zimonjic, D. B., Lowy, D. R., Thorgeirsson, S. S., and Popescu, N. C. (2007) DLC-1: a Rho GTPase-activating protein and tumour suppressor. *J. Cell. Mol. Med.* **11**, 1185-1207
14. Pirone, D. M., Carter, D. E., and Burbelo, P. D. (2001) Evolutionary expansion of CRIB-containing Cdc42 effector proteins. *Trends Genet.* **17**, 370-373
15. Nur-E-Kamal, M. S. A., Kamal, J. M., Qureshi, M. M., and Maruta, H. (1999) The CDC42-specific inhibitor derived from ACK-1 blocks v-Ha- Ras-induced transformation. *Oncogene* **18**, 7787-7793
16. Mott, H. R. and Owen, D. (2015) Structures of Ras superfamily effector complexes: What have we learnt in two decades? *Crit. Rev. Biochem. Mol. Biol.* **50**, 85-133
17. Mott, H. R., Owen, D., Nietlispach, D., Lowe, P. N., Manser, E., Lim, L., and Laue, E. D. (1999) Structure of the small G protein Cdc42 bound to the GTPase-binding domain of ACK. *Nature* **399**, 384-388
18. Tetley, G. J. N., Mott, H. R., Cooley, R. N., and Owen, D. (2017) A dock and coalesce mechanism driven by hydrophobic interactions governs Cdc42 binding with its effector protein ACK. *J. Biol. Chem.* **292**, 11361-11373
19. Odegrip, R., Coomber, D., Eldridge, B., Hederer, R., Kuhlman, P. A., Ullman, C., FitzGerald, K., and McGregor, D. (2004) CIS display: In vitro selection of peptides from libraries of protein-DNA complexes. *Proc. Natl. Acad. Sci. U. S. A.* **101**, 2806-2810
20. McCormick, F. (2018) Targeting KRAS Directly. *Annual Review of Cancer Biology* **2**, 81-90
21. Vetter, I. R., and Wittinghofer, A. (2001) Signal transduction - The guanine nucleotide-binding switch in three dimensions. *Science* **294**, 1299-1304
22. Stephen, A. G., Esposito, D., Bagni, R. K., and McCormick, F. (2014) Dragging Ras Back in the Ring. *Cancer Cell* **25**, 272-281
23. Chakraborty, A., Linnane, E., and Ross, S. (2018) Ras proteins as therapeutic targets. *Biochem. Soc. Trans.* **46**, 1303-1311
24. Futaki, S., Suzuki, T., Ohashi, W., Yagami, T., Tanaka, S., Ueda, K., and Sugiura, Y. (2001) Arginine-rich peptides. An abundant source of membrane-permeable peptides having potential as carriers for intracellular protein delivery. *J. Biol. Chem.* **276**, 5836-5840
25. Wang, K., Qi, J., Weng, T., Tian, Z., Lu, Y., Hu, K., Yin, Z., and Wu, W. (2014) Enhancement of oral bioavailability of cyclosporine A: comparison of various nanoscale drug-delivery systems. *Int J Nanomedicine* **9**, 4991-4999
26. Heard, K. R., Wu, W., Li, Y., Zhao, P., Woznica, I., Lai, J. H., Beinborn, M., Sanford, D. G., Dimare, M. T., Chiluwal, A. K., Peters, D. E., Whicher, D., Sudmeier, J. L., and Bachovchin, W.

- W. (2013) A general method for making peptide therapeutics resistant to serine protease degradation: application to dipeptidyl peptidase IV substrates. *J. Med. Chem.* **56**, 8339-8351
27. Werle, M., and Bernkop-Schnurch, A. (2006) Strategies to improve plasma half life time of peptide and protein drugs. *Amino Acids* **30**, 351-367
28. Martinek, T. A., and Fulop, F. (2012) Peptidic foldamers: ramping up diversity. *Chem. Soc. Rev.* **41**, 687-702
29. Walensky, L. D., and Bird, G. H. (2014) Hydrocarbon-stapled peptides: principles, practice, and progress. *J. Med. Chem.* **57**, 6275-6288
30. Henninot, A., Collins, J. C., and Nuss, J. M. (2018) The Current State of Peptide Drug Discovery: Back to the Future? *J. Med. Chem.* **61**, 1382-1414
31. Tunnemann, G., Ter-Avetisyan, G., Martin, R. M., Stockl, M., Herrmann, A., and Cardoso, M. C. (2008) Live-cell analysis of cell penetration ability and toxicity of oligo-arginines. *J Pept Sci* **14**, 469-476
32. Raagel, H., Saalik, P., and Pooga, M. (2010) Peptide-mediated protein delivery-which pathways are penetrable? *Biochim. Biophys. Acta* **1798**, 2240-2248
33. LeCher, J. C., Nowak, S. J., and McMurry, J. L. (2017) Breaking in and busting out: cell-penetrating peptides and the endosomal escape problem. *Biomol Concepts* **8**, 131-141
34. Tuveson, D. A., Shaw, A. T., Willis, N. A., Silver, D. P., Jackson, E. L., Chang, S., Mercer, K. L., Grochow, R., Hock, H., Crowley, D., Hingorani, S. R., Zaks, T., King, C., Jacobetz, M. A., Wang, L. F., Bronson, R. T., Orkin, S. H., DePinho, R. A., and Jacks, T. (2004) Endogenous oncogenic K-ras(G12D) stimulates proliferation and widespread neoplastic and developmental defects. *Cancer Cell* **5**, 375-387
35. Mahendrarajah, N., Paulus, R., and Kramer, O. H. (2016) Histone deacetylase inhibitors induce proteolysis of activated CDC42-associated kinase-1 in leukemic cells. *J. Cancer Res. Clin. Oncol.* **142**, 2263-2273
36. Mahendrarajah, N., Borisova, M. E., Reichardt, S., Godmann, M., Sellmer, A., Mahboobi, S., Haitel, A., Schmid, K., Kenner, L., Heinzl, T., Beli, P., and Kramer, O. H. (2017) HSP90 is necessary for the ACK1-dependent phosphorylation of STAT1 and STAT3. *Cell. Signal.* **39**, 9-17
37. Tetley, G. J. N., Szeto, A., Fountain, A. J., Mott, H. R., and Owen, D. (2018) Bond swapping from a charge cloud allows flexible co-ordination of upstream signals through WASP: Multiple regulatory roles for the WASP basic region. *J. Biol. Chem.* **293**, 15136-15151
38. Dominguez, C., Boelens, R., and Bonvin, A. (2003) HADDOCK: A protein-protein docking approach based on biochemical or biophysical information. *J. Am. Chem. Soc.* **125**, 1731-1737
39. van Zundert, G. C. P., Rodrigues, J., Trellet, M., Schmitz, C., Kastiris, P. L., Karaca, E., Melquiond, A. S. J., van Dijk, M., de Vries, S. J., and Bonvin, A. (2016) The HADDOCK2.2 Web Server: User-Friendly Integrative Modeling of Biomolecular Complexes. *J. Mol. Biol.* **428**, 720-725
40. Martinez Molina, D., and Nordlund, P. (2016) The Cellular Thermal Shift Assay: A Novel Biophysical Assay for In Situ Drug Target Engagement and Mechanistic Biomarker Studies. *Annu. Rev. Pharmacol. Toxicol.* **56**, 141-161
41. Lawson, C. D., and Ridley, A. J. (2018) Rho GTPase signaling complexes in cell migration and invasion. *J. Cell Biol.* **217**, 447-457
42. Lopez-Mirabal, H. R., and Winther, J. R. (2008) Redox characteristics of the eukaryotic cytosol. *Biochimica Et Biophysica Acta-Molecular Cell Research* **1783**, 629-640

*Inhibition of Ras-Cdc42 signalling by a cyclic peptide*

43. Gilbert, H. F. (1995) Thiol/disulfide exchange equilibria and disulfide bond stability. in *Biothiols, Pt A: Monothiools and Dithiols, Protein Thiols, and Thiyl Radicals* (Packer, L. ed.). pp 8-28
44. Austin, C. D., Wen, X. H., Gazzard, L., Nelson, C., Scheller, R. H., and Scales, S. J. (2005) Oxidizing potential of endosomes and lysosomes limits intracellular cleavage of disulfide-based antibody-drug conjugates. *Proc. Natl. Acad. Sci. U. S. A.* **102**, 17987-17992
45. Santra, S., Kaittanis, C., Santiesteban, O. J., and Perez, J. M. (2011) Cell-Specific, Activatable, and Theranostic Prodrug for Dual-Targeted Cancer Imaging and Therapy. *J. Am. Chem. Soc.* **133**, 16680-16688
46. Galande, A. K., and Spatola, A. F. (2001) A facile method for the direct synthesis of lanthionine containing cyclic peptides. *Letters in Peptide Science* **8**, 247-251
47. Owen, D., and Mott, H. R. (2018) CRIB effector disorder: exquisite function from chaos. *Biochem. Soc. Trans.* **46**, 1289-1302
48. Buck, M., Xu, W., and Rosen, M. K. (2004) A two-state allosteric model for autoinhibition rationalizes WASP signal integration and targeting. *J. Mol. Biol.* **338**, 271-285
49. Cimmerman, P., Baranauskiene, L., Jachimoviciute, S., Jachno, J., Torresan, J., Michailoviene, V., Matuliene, J., Sereikaite, J., Bumelis, V., and Matulis, D. (2008) A quantitative model of thermal stabilization and destabilization of proteins by ligands. *Biophys. J.* **95**, 3222-3231
50. Lim, Y. T., Prabhu, N., Dai, L., Go, K. D., Chen, D., Sreekumar, L., Egeblad, L., Eriksson, S., Chen, L., Veerappan, S., Teo, H. L., Tan, C. S. H., Lengqvist, J., Larsson, A., Sobota, R. M., and Nordlund, P. (2018) An efficient proteome-wide strategy for discovery and characterization of cellular nucleotide-protein interactions. *PLoS One* **13**, e0208273
51. Qian, Z., Martyna, A., Hard, R. L., Wang, J., Appiah-Kubi, G., Coss, C., Phelps, M. A., Rossman, J. S., and Pei, D. (2016) Discovery and Mechanism of Highly Efficient Cyclic Cell-Penetrating Peptides. *Biochemistry* **55**, 2601-2612
52. Hopkins, A. L. (2008) Network pharmacology: the next paradigm in drug discovery. *Nat. Chem. Biol.* **4**, 682-690
53. Zang, M., Hayne, C., and Luo, Z. (2002) Interaction between active Pak1 and Raf-1 is necessary for phosphorylation and activation of Raf-1. *J. Biol. Chem.* **277**, 4395-4405
54. Park, E. R., Eblen, S. T., and Catling, A. D. (2007) MEK1 activation by PAK: a novel mechanism. *Cell. Signal.* **19**, 1488-1496
55. Owen, D., Mott, H. R., Laue, E. D., and Lowe, P. N. (2000) Residues in Cdc42 that specify binding to individual CRIB effector proteins. *Biochemistry* **39**, 1243-1250
56. Owen, D., Lowe, P. N., Nietlispach, D., Brosnan, C. E., Chirgadze, D. Y., Parker, P. J., Blundell, T. L., and Mott, H. R. (2003) Molecular dissection of the interaction between the small G proteins Rac1 and RhoA and protein kinase C-related kinase 1 (PRK1). *J. Biol. Chem.* **278**, 50578-50587
57. Campbell, L., Peppas, M., Crabtree, M., Shafiq, A., McGough, N., Mott, H.R. and Owen, D. . (2015) Thermodynamic Mapping of Effector Protein Interfaces with RalA and RalB. *Biochemistry* **54**, 1380-1389
58. Elliot-Smith, A. E., Owen, D., Mott, H. R., and Lowe, P. N. (2007) Double mutant cycle thermodynamic analysis of the hydrophobic Cdc42-ACK protein-protein interaction. *Biochemistry* **46**, 14087-14099
59. R Core Team: R Foundation for Statistical Computing, V., Austria. (2018) R: A language and environment for statistical computing.

*Inhibition of Ras-Cdc42 signalling by a cyclic peptide*

60. Vranken, W. F., Boucher, W., Stevens, T. J., Fogh, R. H., Pajon, A., Llinas, P., Ulrich, E. L., Markley, J. L., Ionides, J., and Laue, E. D. (2005) The CCPN data model for NMR spectroscopy: Development of a software pipeline. *Proteins-Structure Function and Bioinformatics* **59**, 687-696
61. Linge, J. P., O'Donoghue, S. I., and Nilges, M. (2001) Automated assignment of ambiguous NOEs with ARIA. *Methods Enzymol.* **339**, 71-90
62. Brunger, A. T., Adams, P. D., Clore, G. M., DeLano, W. L., Gros, P., Grosse-Kunstleve, R. W., Jiang, J. S., Kuszewski, J., Nilges, M., Pannu, N. S., Read, R. J., Rice, L. M., Simonson, T., and Warren, G. L. (1998) Crystallography & NMR system: A new software suite for macromolecular structure determination. *Acta Crystallographica Section D-Biological Crystallography* **54**, 905-921
63. Hubbard, S. J. T., J.M. (1993) NACCESS. Department of Biochemistry and Molecular Biology, University College London
64. Rueden, C. T., Schindelin, J., Hiner, M. C., DeZonia, B. E., Walter, A. E., Arena, E. T., and Eliceiri, K. W. (2017) ImageJ2: ImageJ for the next generation of scientific image data. *BMC Bioinformatics* **18**, 529
65. Schindelin, J., Arganda-Carreras, I., Frise, E., Kaynig, V., Longair, M., Pietzsch, T., Preibisch, S., Rueden, C., Saalfeld, S., Schmid, B., Tinevez, J. Y., White, D. J., Hartenstein, V., Eliceiri, K., Tomancak, P., and Cardona, A. (2012) Fiji: an open-source platform for biological-image analysis. *Nat Methods* **9**, 676-682

**Footnotes**

**Abbreviations:** ACK, activated Cdc42 kinase; CETSA, cellular thermal shift assays; CRIB, Cdc42/Rac interactive binding domain; CPP, cell penetrating peptide; DTT, dithiothreitol; FAM, carboxyfluorescein; FITC, fluorescein-5,6-isothiocyanate; GAP, GTPase activating protein; GBD, G protein binding domain; GDP, guanosine-5'-diphosphate; GEF, guanine exchange factor; GST, glutathione-S-transferase; GTP, guanosine-5'-triphosphate; IPTG, isopropyl- $\beta$ -D-1-thiogalactopyranoside; MEF, mouse embryonic fibroblast; PAK, p21 activated kinase; SPA, scintillation proximity assay; WASP, Wiskott-Aldrich syndrome protein; wt, wildtype; 9R, nona-arginine.

**Table 1: Experimental Restraints and Structural Statistics <sup>a</sup>**

**Experimental restraints**

Distance restraints:

Total non-degenerate	440
Unambiguous	408
Ambiguous	32
Intraresidue NOEs	170
Sequential NOEs	115
Medium & long-range NOEs	155

	<SA> <sup>b</sup>	<SA> <sup>c</sup>
<b>Coordinate precision for well-ordered regions</b>		
RMSD of all backbone atoms (Å)	0.37 ± 0.13	0.15
RMSD of all heavy atoms (Å)	0.69 ± 0.09	0.63
<b>RMS deviations for all residues</b>		
from the experimental restraints:		
NOE distances (Å)	0.025 ± 0.0014	0.025
from idealised geometry:		
Bonds (Å)	0.0045 ± 0.00023	0.0044
Angles (°)	0.83 ± 0.025	0.83
Impropers (°)	1.30 ± 0.17	1.18
<b>Ramachandran plot analysis <sup>d</sup></b>		
Core region (%)	59.5	50.0
Allowed region (%)	30.7	41.7
Generously allowed region (%)	9.0	8.3
Disallowed region (%)	0.7	0.0

<sup>a</sup> PDB accession code 6R28. Chemical shifts deposited at BMRB, accession code 34380.

<sup>b</sup> <SA> represents the average RMS deviations for the ensemble of 36 structures.

<sup>c</sup> <SA> represents values for the structure that is closest to the mean.

<sup>d</sup> Analysed using Procheck

**Table 2:** Affinities of peptides for a panel of small G proteins measured by FP.

	$K_d$ (nM) $\pm$ standard deviation		
	<b>C1</b>	<b>P1</b>	<b>P7</b>
Cdc42·GDP	876.0 $\pm$ 170.0	98.4 $\pm$ 9.1	32.0 $\pm$ 4.3
Cdc42·GMPPNP	409.0 $\pm$ 44.2	24.5 $\pm$ 8.6	14.6 $\pm$ 3.4
Rac1·GMPPNP	355.0 $\pm$ 79.0	896.0 $\pm$ 123.0	436.0 $\pm$ 107.0
RhoA·GMPPNP	475.0 $\pm$ 152.0	166.0 $\pm$ 52.2	ND*
K-Ras 4B·GMPPNP	3418.0 $\pm$ 581.0	3970.0 $\pm$ 614.0	19600.0 $\pm$ 5600.0
RalA·GMPPNP	44000.0 $\pm$ 1251.0	37040.0 $\pm$ 1340.0	ND

\* ND (no binding) denotes data that could not be fitted to the binding isotherm

## Figure Legends

**Figure 1 A:** Bar charts showing the relative enrichment of peptides in each library pool and the ten most frequently selected sequences under each set of conditions. Sequences taken forward for further evaluation are highlighted in red. **B:** ELISA screening of phage presenting the three most enriched sequences. The relative absorbances from ELISA for binding against a panel of small GTPase targets as indicated and a BSA control are plotted as a modified box plot.  $n = 3-4$  **C:** Displacement of [ $^3\text{H}$ ]GTP·Cdc42 from GST-wt ACK GBD by C1 binding to Cdc42. Increasing concentrations of C1 or C1<sup>C4S, C13S</sup> were titrated into a fixed concentrations of [ $^3\text{H}$ ]GTP·Cdc42 and GST-wt ACK GBD in the presence or absence of 50 mM DTT, in competition SPAs. The  $K_d$  for Cdc42 binding to GST-wt ACK GBD was fixed to the value (30 nM) obtained for this  $K_d$  in direct SPAs. The data were fitted to an isotherm describing a pure competition model (58) to give an apparent  $K_d$  ( $K_i$ ) value for C1. The data and curve fits are displayed as a percentage of the maximal SPA signal in each assay.

**Figure 2 A:** The affinity of C1 and FAM-C1-9R for Cdc42. The top panel shows anisotropy data for direct binding of 60 nM FAM-C1-9R or FAM-9R to varying concentrations of Cdc42·GMPPNP with data fitted to a direct binding model containing a linear non-specific-binding term.  $n = 3$ . The bottom panel shows the competition between 60 nM FAM-C1-9R and 500 nM Cdc42·GMPPNP with a range of concentrations of unmodified C1, fitted to a competition binding model to calculate binding affinity.  $n = 2$  **B:** The effect of higher concentrations of FAM-C1-9R on cells. MEFs treated with peptide or a FITC control for varying times are shown under 20X phase contrast. After 28 hours cells were washed twice in PBS and imaged by phase contrast, and fluorescence using an EVOS GFP light cube. These images are shown in overlay in the bottom panels. **C:** Entry of FAM-C1-9R into cells. Peptide at 5 different concentrations was applied to MEFs and the cells monitored by fluorescence confocal microscopy at 4 different time-points. Representative images are shown and labeled accordingly.  $n = 3$ . **D:** Effects of the peptides on signalling pathways. MEFs were incubated with FAM-C1-9R for 1 and 24 hours alongside untreated controls (0). Cell lines A and C expressed K-Ras G12D while B and D were wild type. Western blots from whole cell lysate were probed for Stat3 phospho-Tyr705, total Stat3, ERK1/2 phospho-Thr202/204, total ERK1/2 and GAPDH. Data are representative of three independent experiments.

**Figure 3 A:** The enrichment of replacement residues in second generation peptides after maturation by CIS display. At positions where the parent residue was proportionately decreased in abundance after 4 rounds of biopanning of the cyclic maturation library, the relative enrichment of replacement residues at each amino acid is shown in the bar chart. Amino acids are individually coloured as shown in the key and labelled using one letter code where they have a greater than 2-fold enrichment. **B:** Second generation peptides. The nine selected sequences from the maturation screen are presented. Their affinities for Cdc42·GTP were determined by competition SPA and their  $K_d$ s are given together with the standard error from curve fitting.  $n \geq 2$ . **C:** Representative SPA data. Increasing concentrations of the ACK GBD or the peptides were titrated into a fixed concentrations of [ $^3\text{H}$ ]GTP·Cdc42 and GST-wt ACK GBD in competition SPAs. The  $K_d$  for Cdc42 binding to GST-wt ACK GBD was fixed to the value (30 nM) obtained for this  $K_d$  in direct SPAs. The data were fitted to an isotherm describing a pure competition model(58) to give an apparent  $K_d$  ( $K_i$ ) value for the peptides. The data and curve fits are displayed as a percentage of the maximal SPA signal in each assay.

**Figure 4:** Structural analysis of peptide P7 and its interactions with Cdc42. **A.** HSQC spectra of <sup>15</sup>N-labelled Cdc42 in its free (black) and bound (red) forms. The peaks corresponding to the free form are labelled with their assignment in one letter code and are connected by a blue line to the corresponding resonance in the bound form. Peaks that had shifted too far to be reliably assigned are labelled in blue. **B.** A surface representation of Cdc42 with those residues that experienced a larger than average shift change and which were more than 50% solvent exposed coloured orange. **C.** The family of structures of peptide P7 is shown in green with the disulphide bond in yellow. Side chain nitrogen atoms are in blue and oxygen atoms are in red (PDB accession code 6R28). The sidechains are well defined in the structures with the exception of the C-terminal Arg16 and the two residues in the loop, Arg8 and Asp10, which are responsible for high affinity binding of this peptide. **D.** A backbone representation of the closest structure to the mean.

**Figure 5:** **A.** Data-driven model of the Cdc42-peptide P7 complex generated using *HADDOCK*. Peptide P7 is shown in green with the disulphide bond in yellow and Cdc42 is blue with the nucleotide shown in a stick representation. Residues identified from the chemical shift mapping are depicted as coloured spheres: those that had shifted the most (more than average + 1 standard deviation) are coloured red, those that had shifted by more than average but less than average + 1 S.D are coloured yellow and those that had shifted too far to reliably assign are coloured orange. **B.** The Cdc42-P7 model shown in the same orientation as in panel A in a surface representation. P7 is shown in green and Cdc42 in blue. The peptide binds in a Cdc42 pocket between the β2-β3 hairpin and helix α5, which is lined by residues that showed chemical shift changes upon peptide binding. **C.** A close-up of some of the interactions in the model indicates that Arg8, Asp10, Trp11 and Tyr15 of the peptide loop insert into the Cdc42 pocket and that salt bridges form between Asp10<sup>P7</sup> and Lys166<sup>Cdc42</sup> and Arg8<sup>P7</sup> and Tyr23<sup>Cdc42</sup>.

**Figure 6:** The P7 binding site overlaps with the binding surface of the CRIB effectors on Cdc42. ACK, PAK1, WASP and the Par6 semi-CRIB all form contacts with the same pocket so that the peptide binding will cause steric clashes with CRIB effectors. Cdc42 is shown as a blue cartoon, peptide P7 (green) and the CRIB effectors (shades of pink) are shown as a semi-transparent surface overlaid on cartoons.

**Figure 7:** The affinities of peptides FAM-C1-9R, FAM-P1-9R and FAM-P7-9R for a panel of small GTPases were measured by FP. The  $K_d$ s (see also Table 1), determined from  $n \geq 3$  assays, are plotted as reciprocals on a radar chart to demonstrate the relative affinity of the peptides for small GTPases related to Cdc42. Units of  $1/K_d = \mu\text{M}^{-1}$ .

**Figure 8 A.** Entry of FAM-9R conjugated peptides into A549 cells. Peptides were applied to A549 cells at a final concentration of 1 μM and the cells monitored by confocal microscopy at a variety of time-points. Representative images are shown and labeled accordingly. **B:** Inhibition of Cdc42-effector interactions by C1 and second generation peptides (P1 and P7). The ability of Cdc42 to interact with its effector WASP in A549 lysate was monitored by GST-WASP pulldown experiments. GST-WASP GBD immobilized on glutathione agarose beads was used to pull down endogenous Cdc42 from A549 lysates in the presence of various peptide concentrations. The levels of Cdc42 bound were analysed by western blot. Representative western blots from unconjugated C1, P1 and P7 treatments are shown in the upper panels. Densitometry was performed on the results from replicate experiments ( $n \geq 3$ ) and the amount of

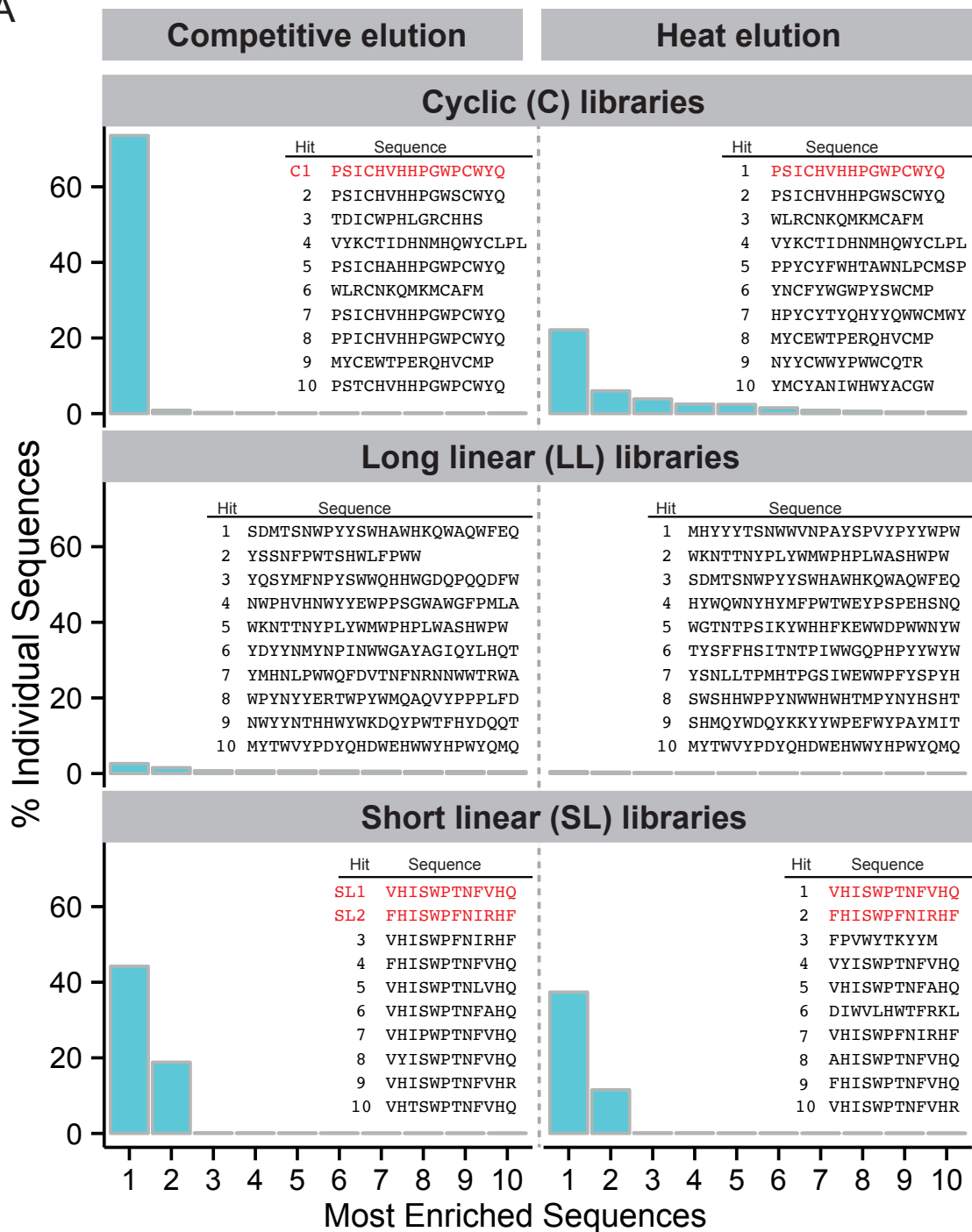
### *Inhibition of Ras-Cdc42 signalling by a cyclic peptide*

Cdc42 present in pulldowns, expressed as a percentage of levels in the absence of peptides, are plotted in the lower panel. Data for FAM-9R conjugated peptides are also included. C1, pink; FAM-C1-9R, red; P1, green; P7, cyan; FAM-P7-9R, purple. Approximate IC<sub>50</sub>s were calculated from the curve fits: C1, 190 ± 62 nM; FAM-C1-9R, 2200 ± 740 nM; P1, 18 ± 3.5 nM; P7, 1.2 ± 0.28 nM, FAM-P7-9R, 65 ± 12 nM. **C:** Target engagement by peptides. Cellular thermal stability assays (CETSA) were run in A549 lysate at 56 °C treated with varying concentrations of FAM-P7-9R peptide to assess target engagement. Cdc42 and actin (as a control) levels were quantified by western blot and a representative blot is presented showing destabilization of Cdc42 with increasing peptide concentration. n = 3. **D:** Target engagement after cell penetration. Whole cell CETSA experiments were run in A549 cells at 51 °C after 4 h incubation with varying concentrations of FAM-P7-9R peptide to assess target engagement after external application of peptide. After lysis Cdc42 and actin levels were quantified by western blot and a representative blot is presented showing destabilization of Cdc42 with increasing peptide concentration. n = 3.

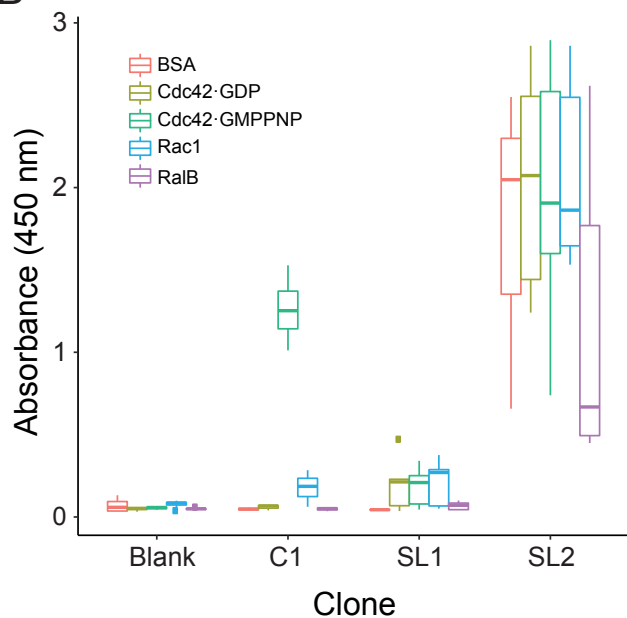
**Figure 9 A:** Peptide effects on proliferation of A549 cells. The proliferation of A549 cells was analyzed over 48 hours by MTT assay. Proliferation data are shown for 48 h timepoints from 6-12 replicate experiments at three different peptide concentrations. A<sub>570</sub> values are shown as a proportion of the untreated control values and displayed as modified boxplots. Group significance testing at each dosing level was performed by T-test (n = 12 - 34): #, p < 0.1; \*, p < 0.05; \*\*, p < 0.01. **B:** Peptide effects on migration and invasion of A549 cells. Boyden chamber assays were used to assess cell migration and invasion. Cells were seeded in the top chamber in 0.1% serum and migration through the membrane to 10% serum containing media measured. Cell numbers relative to untreated control cells are shown as modified boxplots and a significant decrease in proliferation relative to 9R was assessed using the one-way T-test (n = 4): #, p < 0.1; \*, p < 0.05. **C:** Peptide effects on proliferation and migration of A549 cells. Scratch assays were used to measure cell proliferation and co-ordinated migration. Representative images over the first 24 hours of the assay are shown for each of the peptides in the left hand panels. The complete data set (n=3) is shown in the graph (right hand panel) with the percentage area of the scratch left uncovered by cells for each condition plotted at each time point, with error bars representing the standard error of the mean.

Figure 1

A



B



C

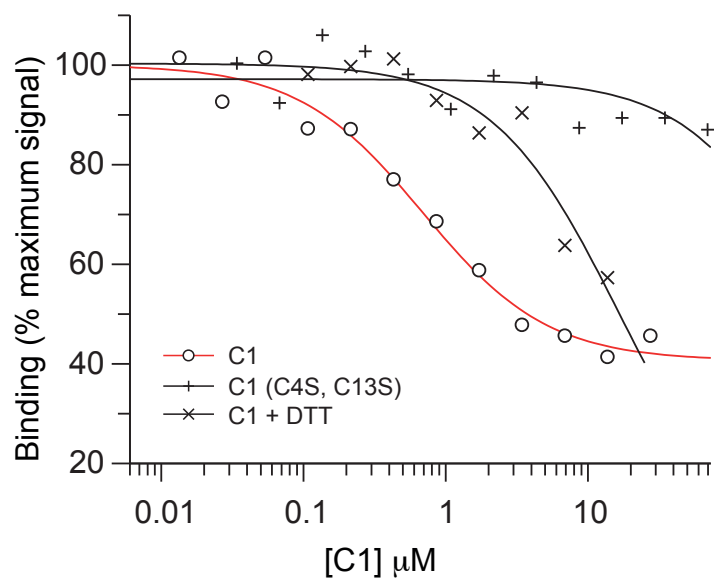
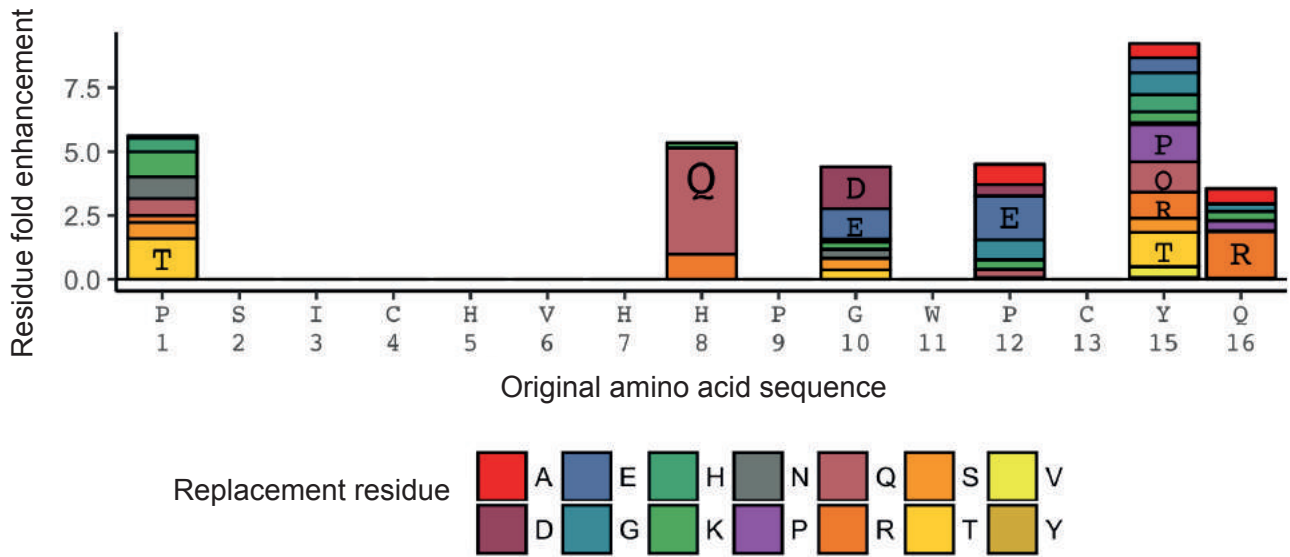




Figure 3

A



B

Peptide	Sequence	$K_d$ (nM) <sup>1</sup>
C1	P S I C H V H H P G W P C W Y Q	420 ± 153
P1	T S I C H V H Q P G W P C W Y R	24 ± 7
P2	T S I C H V H H P G W P C W Y Q	732 ± 113
P3	P S I C H V H Q P G W P C W Y Q	560 ± 115
P4	P S I C H V H H P G W P C W Y R	516 ± 330
P5	P S I C H V H R P D W P C W Y Q	32 ± 4
P6	T S I C H V H R P D W P C W Y Q	32 ± 7
P7	P S I C H V H R P D W P C W Y R	24 ± 5
P8	P S I C H V H Q P S W P C W Y Q	359 ± 111
P9	T S I C H V H Q P S W A C W S R	83 ± 11
	1 2 3 4 5 6 7 8 9 10 11 12 13 14 15 16	

<sup>1</sup> Standard error from curve fitting

C

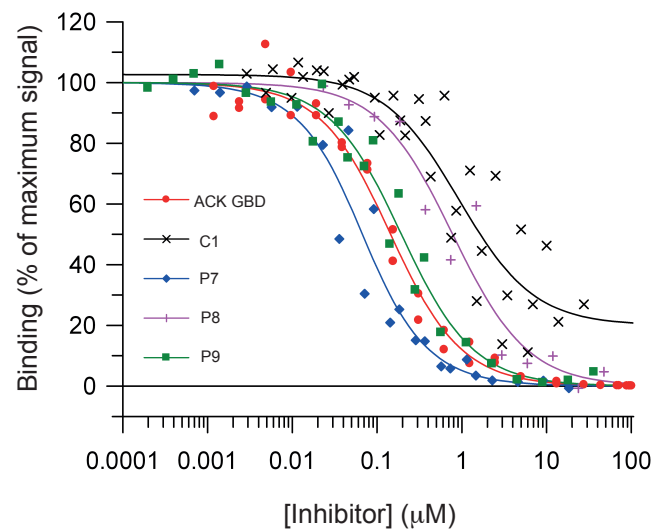
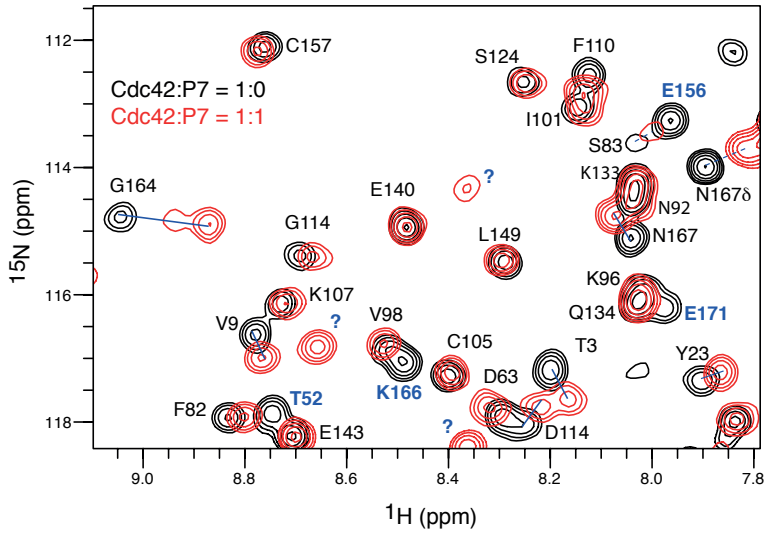
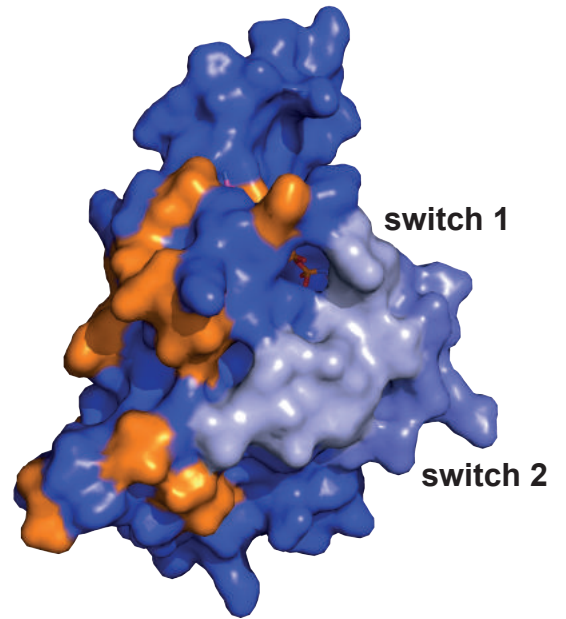


Figure 4

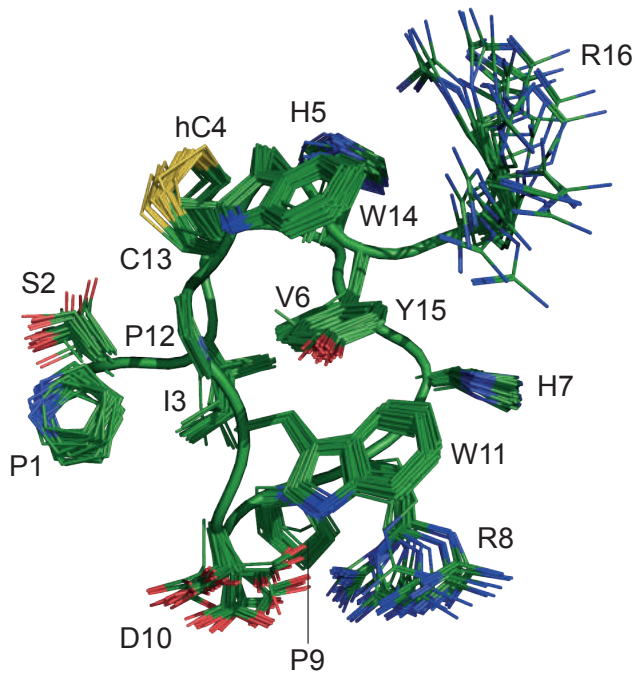
A



B



C



D

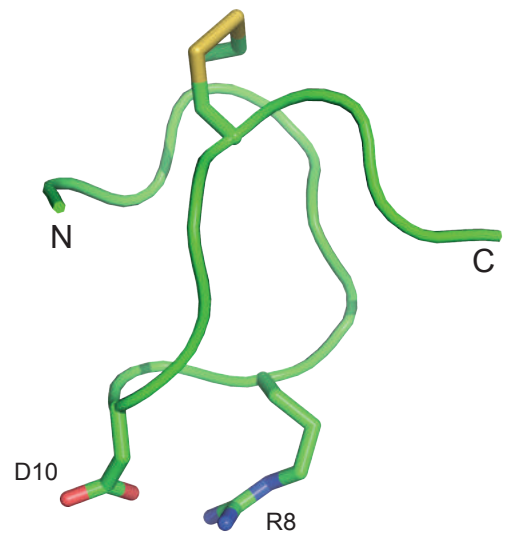


Figure 5

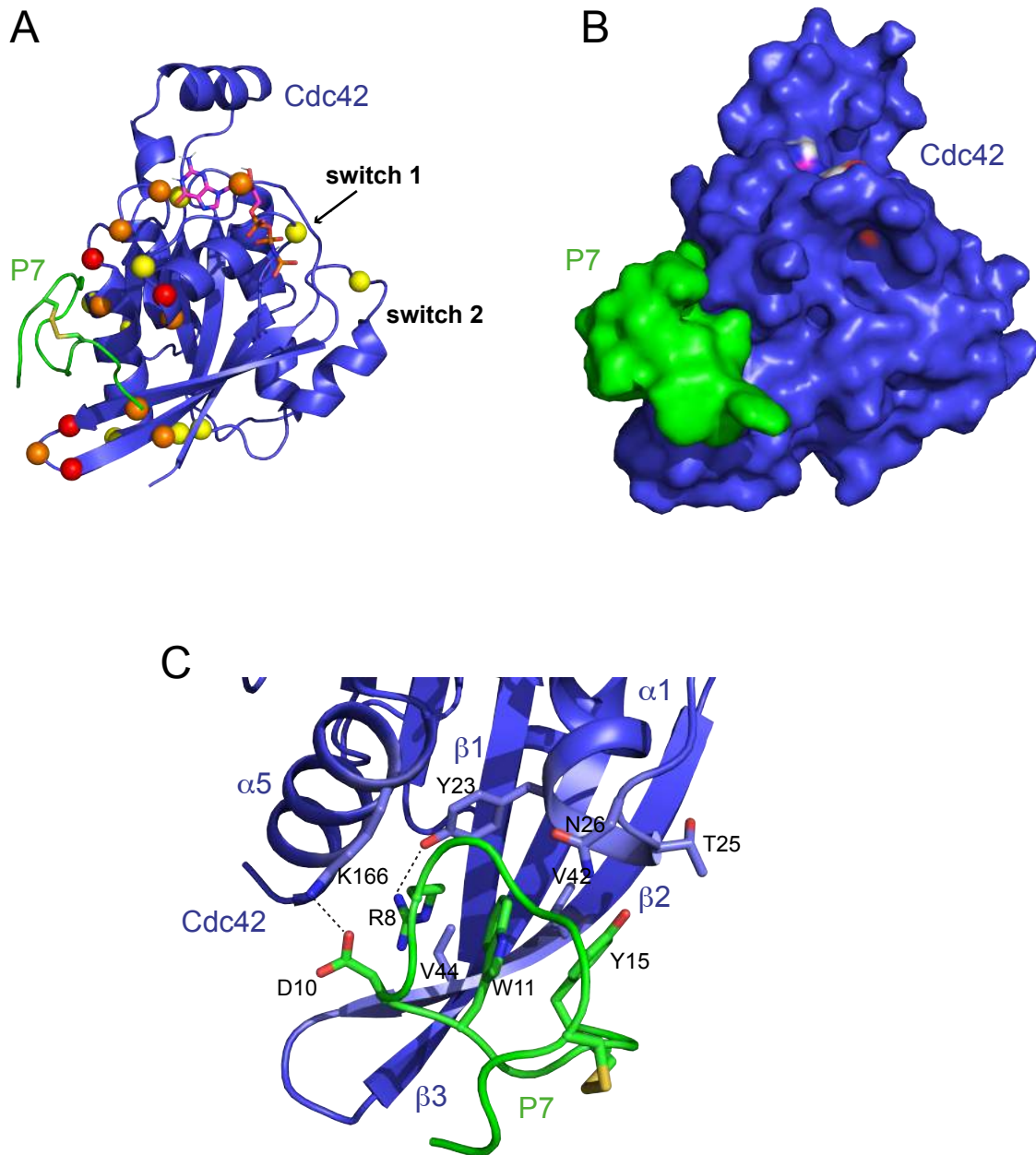


Figure 6

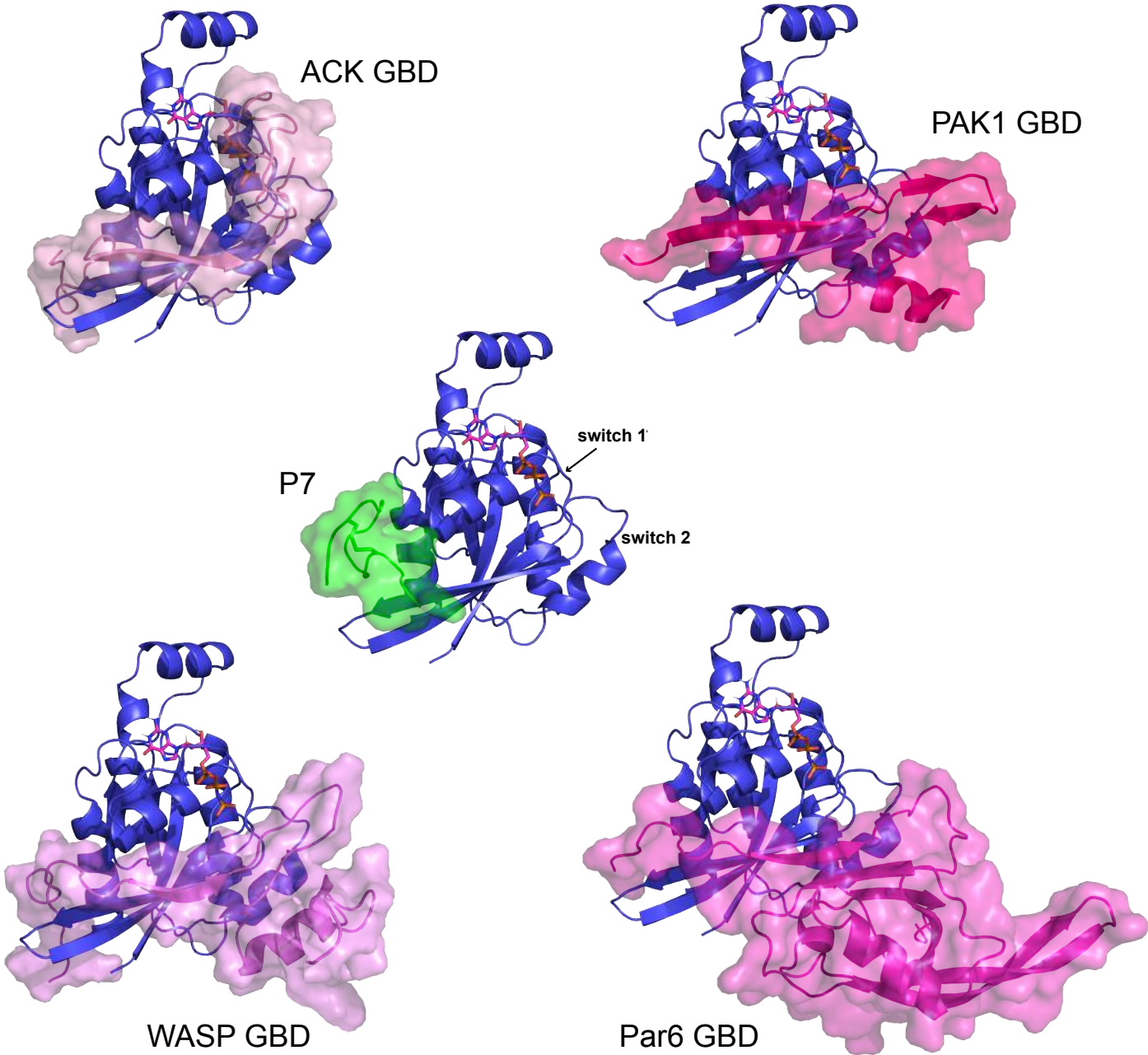


Figure 7

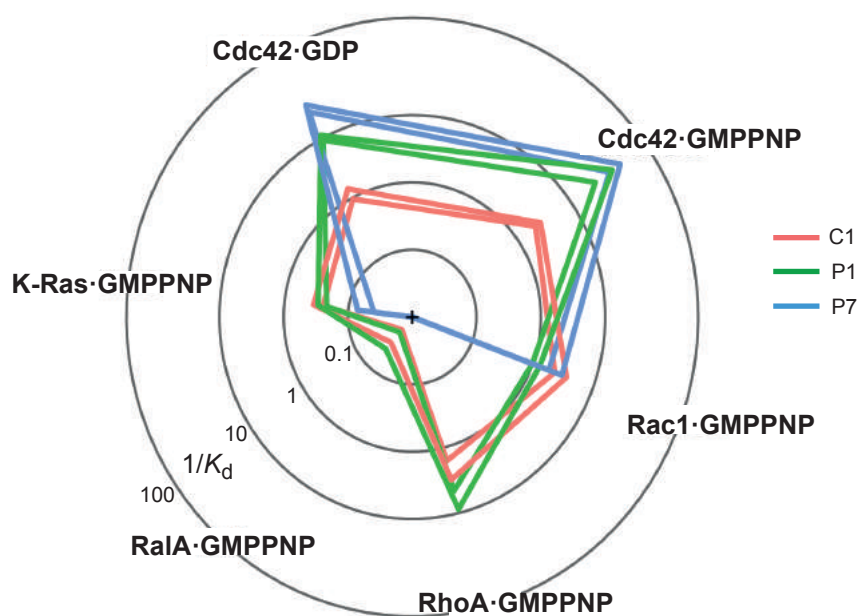


Figure 8

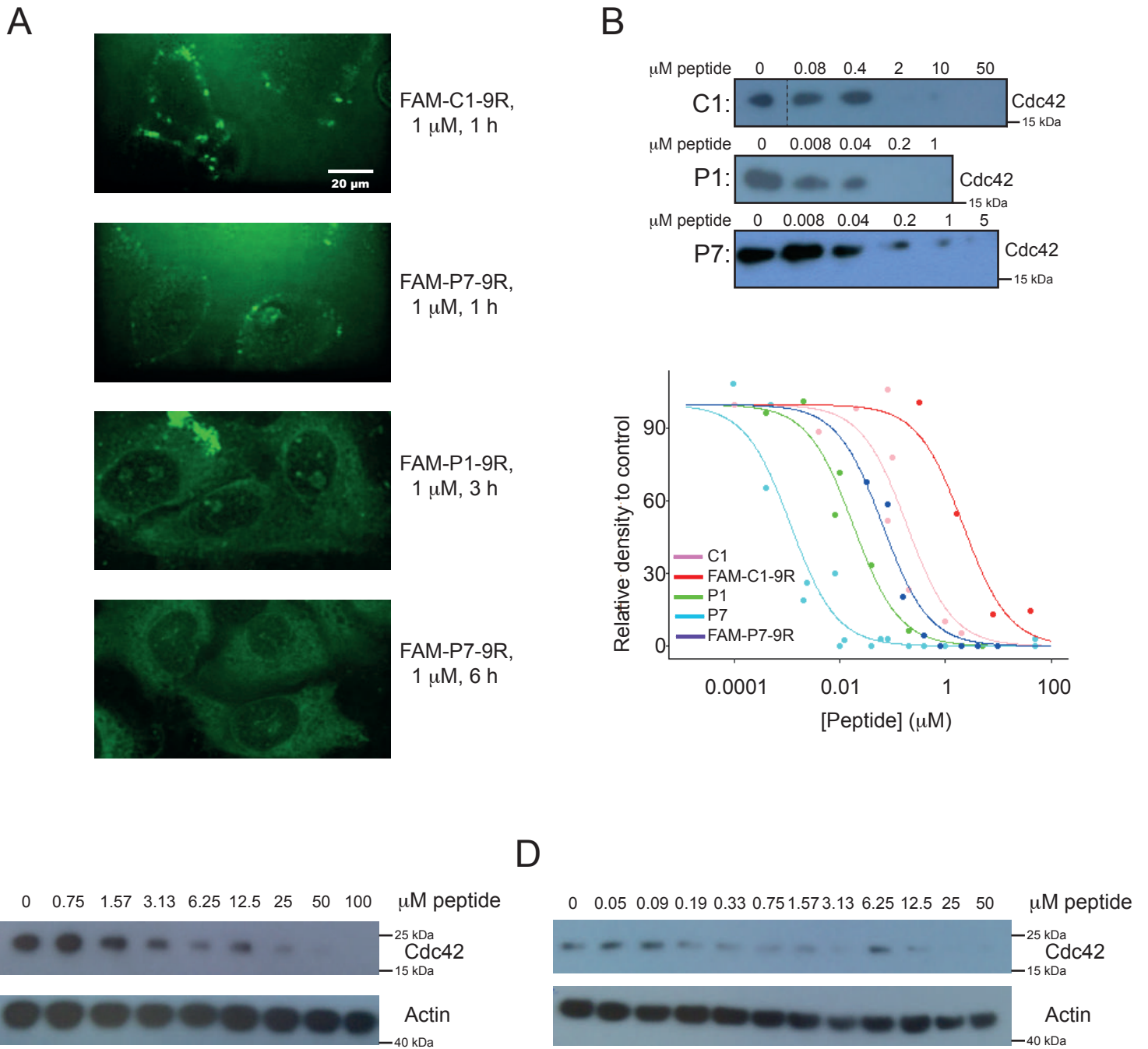
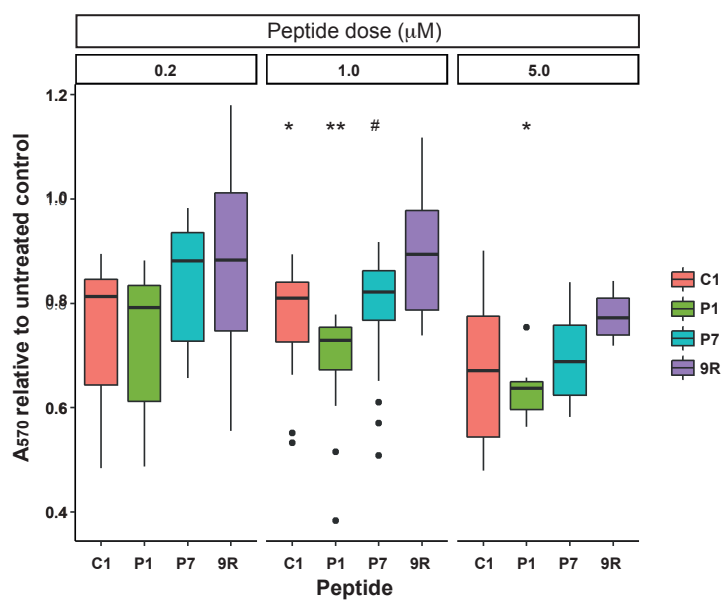
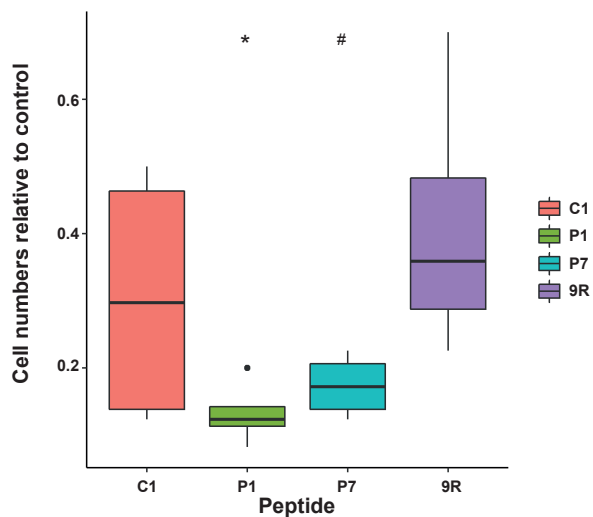


Figure 9

A



B



C

